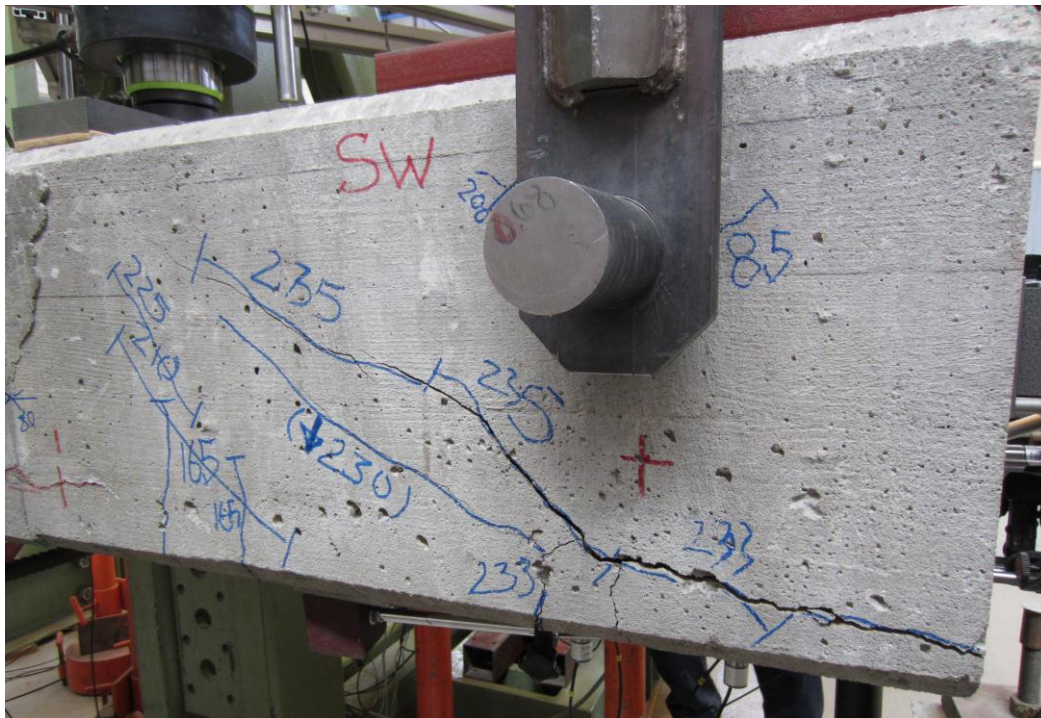# CHALMERS

Bond Behaviour of Naturally Corroded Reinforcement in Concrete Structures

Experimental and Numerical Study

Master of Science Thesis in the Master's Programme Structural Engineering and Building Performance Design

EYRÚN GESTSDÓTTIR
TÓMAS GUÐMUNDSSON

Bond Behaviour of Naturally Corroded Reinforcement in Concrete Structures

Experimental and Numerical Study

Master of Science Thesis in the Master's Programme

EYRÚN GESTDÓTTIR

TÓMAS GUÐMUNDSSON

Department of Civil and Environmental Engineering
Division of Structural Engineering
Concrete Structures
CHALMERS UNIVERSITY OF TECHNOLOGY
Göteborg, Sweden 2012

Bond Behaviour of Naturally Corroded Reinforcement in Concrete Structures
Experimental and Numerical Study

Master of Science Thesis in the Master's Programme Structural Engineering and Building Performance Design

EYRÚN GESTSDÓTTIR

TÓMAS GUÐMUNDSSON

Cover:
South West side of specimen M9 during testing. Photograph taken by Eyrún Gestsdóttir: 3. May 2012.

Bond Behaviour of Naturally Corroded Reinforcement in Concrete Structures
Experimental and numerical study

Master of Science Thesis in the Master's Programme Master of Science Thesis in the Master's Programme Structural Engineering and Building Performance Design

EYRÚN GESTSDÓTTIR
TÓMAS GUÐMUNDSSON
Department of Civil and Environmental Engineering
Division of Structural Engineering
Concrete Structures
Chalmers University of Technology

ABSTRACT

Corrosion of reinforcement is one of the most common causes of deterioration in reinforced concrete structures. When reinforcement corrodes, the bond between the steel and the concrete deteriorates, threatening the structural integrity of the structure. Most of our knowledge about corroded reinforcement has been gained from experimental data where the reinforcement has been corroded accelerated in artificial conditions. There are reasons to believe that artificially corroded reinforced concrete specimens are not behaving in the same way as the specimens which corroded for a long time in a natural environment do. Therefore, it is important to investigate and perform experiments on naturally corroded specimens in order to gain a better understanding of the difference between naturally and artificially corroded specimens. In this thesis naturally corroded specimens from Stallbackabron in Trollhättan, Sweden were investigated, prepared and tested with regard to anchorage capacity. The specimens had different extent of damage caused by corrosion, from no visible cracking to spalling of the concrete. The specimens were tested in four point bending tests, with indirect supports. The relative displacements of the reinforcement bars that were in tension were measured to investigate the bond slip between the reinforcement steel and the concrete. To gain a better understanding of the structural behaviour of the specimens, a non-linear 2D plane stress FE model was developed in the finite elements software DIANA, together with the pre- and post-processor FX+. The results from the FE analysis were compared with the experimental results.

The experiments showed that higher degree of corrosion leads to decrease of ultimate load and longer available anchorage length leads to increase of ultimate load. Furthermore the ultimate load is not connected at what load shear or flexural crack forms. The 2D FE analyses showed good correlation between ultimate load and maximum deflection but could not to full extent describe be behaviour of free end slip or crack pattern. Furthermore it is important to modify the material parameters to get better correspondence to real behaviour of the test specimens.

Key words: Natural corrosion, reinforcement, concrete, anchorage, non-linear finite element method, experiments.

Contents

Preface

In this thesis, bond behaviour of naturally corroded reinforcement in concrete is studied. The work was carried out from December 2011 to June 2012 at the Department of Civil and Environmental Engineering, Division of Structural Engineering, Concrete Structures at Chalmers University of Technology.

Four point bending tests were done on several test specimens originated from Stallbackabron in Trollhättan, to capture an anchorage failure of naturally corroded concrete members. Furthermore, non-liner 2D FE analyses were carried out and the results were compared to the test results.

The authors would like to thank our examiner Professor Karin Lundgren, M. Sc. Mohammad Tahershamsi and Associate Professor Mario Plos for their supervision and for the stimulating/encouraging discussions we had regarding the thesis. Furthermore, we would like to thank Ph.D. Kamyab Zandi Hanjari for his remarkable help with our FE model and for his helpful comments on our results.

We would also like to thank our opponents, Hao Du and Ning Chen for their comments and good advice.

Big part of this thesis was experimental work done with the guidance of Lars Wahlström, Engineer at the Laboratory of Structural Engineering at Chalmers University of Technology. His expertise and experience in the lab has been invaluable to us.

Göteborg, June 2012

Eyrún Gestsdóttir

Tómas Guðmundsson

Notations

Roman upper case letters

E_{cm}	Mean Young's modulus of concrete
E_s	Young's modulus of reinforcement
G_f	Fracture energy of concrete
S	Bond slip
S_1	Bond slip at maximum bond stress
S_2	Bond slip at maximum bond stress in case of pull out failure
S_3	Bond slip at bond failure
N	Normal force

Roman lower case letters

f_{ctm}	Mean tensile strength of concrete
f_{cm}	Mean compressive of concrete
f_{cc}^{d}	Cylinder compressive strength of damaged concrete
f_{sy}	Yield strength of reinforcement
f_{su}	Ultimate strength of reinforcement
s_1	Bond slip at maximum bond stress
s_2	Bond slip at maximum bond stress in case of pull out failure
s_3	Bond slip at bond failure

Greek letters

α	Exponent for ascending bond stress
τ	Bond stress
τ_{max}	Maximum bond stress
τ_f	Bond stress at failure
ε_{sy}	Yield strain of reinforcement
ε_{su}	Ultimate strain of reinforcement

1 Introduction

1.1 Background

Corrosion of steel reinforcement is one of the most common causes of deterioration in reinforced concrete structures. Up until now, most investigations have been performed on artificially corroded specimens.

Corrosion of steel reinforcement decreases the steel area and the bond between the steel and the concrete. The latter is the study of this thesis. When steel corrodes the outermost steel will turn into rust. Rust is bigger in volume than steel and causes therefore stresses in the concrete that eventually will lead to cracking of the concrete. Cracking of the concrete causes loss of confinement for the reinforcement which reduces the bond. Anchorage capacity describes how well the steel reinforcement is anchored into the concrete and is determined by the bond between the reinforcement steel and the concrete itself.

From 2000, effects of corrosion have been studied at Chalmers University of Technology. Berg and Johansson wrote a master thesis about design of a test setup using FEM, a pilot thesis on anchorage of naturally corroded reinforcement in the spring 2011. They aimed at designing a test setup to get an anchorage failure of naturally corroded reinforcement in concrete beams from Stallbackabron in Trollhättan, Sweden. A test setup to capture the anchor failure of the steel was successfully designed and confirmed with a test from the south cantilever of the bridge.

1.2 Aim, method and limitations

The aim of this thesis was to gain better understanding of the structural effects of naturally corroded reinforcement, and especially to investigate bond in naturally corroded concrete structures. In order to achieve that, several beams from the north part of Stallbackabron were tested, with regard to anchorage capacity. The experimental work included the preparations of the test specimens, carrying out the tests and evaluation of the test results. A 2D FE model was developed, that captured the same failure as the beams, to prepare for the testing and also to get a better understanding of the test results through comparison. Emphasis will be on how a 2D model will describe an anchorage failure so a 3D model will not be considered.

1.3 Outline of contents

Chapter 2 gives an overview of the bond behaviour of steel reinforcement. Chapter 3 consists of description of the test specimens, the test setup, steel and concrete material properties. Furthermore, preparations of the specimens and the experiments themselves are described. The choice of non-linear finite element model is described in Chapter 4. The analysis and results are presented in Chapter 5 and they are discussed and conclusions drawn in Chapter 6.

2 Bond behaviour of corroded ribbed bars

Concrete is rather strong in compression but weak in tension. To compensate for that concrete is reinforced with steel to resist bending and shear forces applied on concrete structures. Together concrete and the reinforcing steel act as a composite section. The longitudinal forces are transferred from the steel to the surrounding concrete by the bond between the two materials. The reinforcement has to be carefully anchored in the concrete otherwise it does not interact with the concrete and tensile stresses are not build up within the steel. A certain transmission length has to be applied in order for the steel to bond with the concrete. This length is usually called anchorage length. The relative displacement between the reinforcement bar and the surrounding concrete is called slip.

2.1 Bond between concrete and reinforcement

Bond between ribbed reinforcement steel bars and concrete consists of chemical adhesion, friction and mechanical interlock. Those restraint mechanisms are well known due to a large amount of research performed in the last 40 years. Bond properties are influenced by many aspects and those who have studied it agree that bond between steel and concrete in pull-out can be divided into four different stages, FIB (2000).

 Stage I is when the concrete is still uncracked, then the bond stress values are low, $\tau \leq 0{,}2$-$0{,}8$ f_{ct}. The bond is mainly obtained by weak chemical reaction between the steel and hardened cement. At this stage no bar slip occurs but highly localized stresses arise at the tip of the rib on the bar. Although no bar slip occurs there can be some relative displacement of the bar, see FIB (2000).

Stage II is when the first crack appears, the bond stress values are higher, $\tau > 0{,}2$-$0{,}8$ f_{ct}. The chemical adhesion breaks down and the bond is provided by friction. High stresses at the top of the ribs cause the concrete to crush locally and micro cracks form. However the wedge actions, that is the ribs pushing against the surrounding concrete, at the top of the rib remains limited and there are no signs of concrete splitting, see FIB (2000).

Stage III is for higher bond values, $\tau > 1$-3 f_{ct}. The stresses and the wedge action rise. The stress component on the rib can be split into two components, longitudinal bond stress component causing the transverse cracks and normal stress component causing longitudinal cracks to form, this is the cause of concrete splitting, it can be seen on figure 2.1. The tensile force is resisted by circumferential tensile stresses in the concrete, see Tepfers (1973). The bond strength and stiffness are assured mostly by interlocking action between the reinforcement and the concrete and secondly by friction, see FIB (2000).
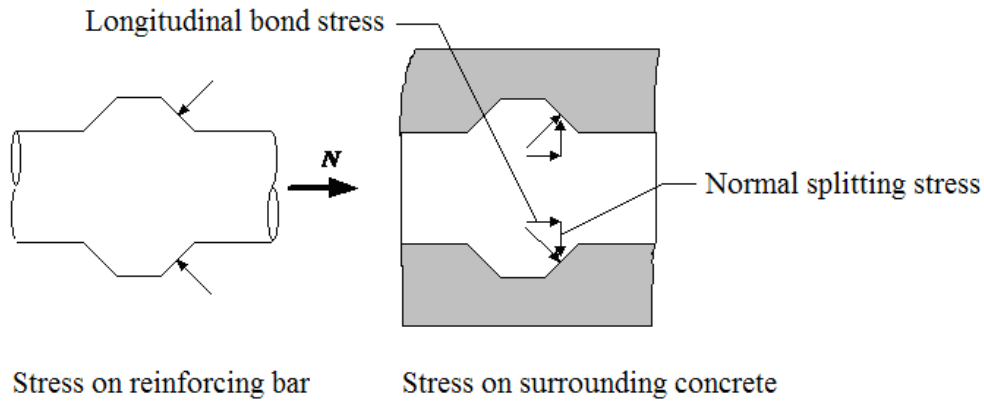
Figure 2.1   Bond between a ribbed bar and the surrounding concrete by mechanical interlocking, from Magnusson (2000) modified by Berg and Johansson (2011).

Stage IV leads to pull-out or splitting failure. Many factors can influence the type of failure. They can be: the degree of confinement, transverse reinforcements, and size of concrete cover and diameter of reinforcement bars. Splitting failure occurs when radial stresses causes longitudinal cracks that propagate up to the surface, it is typical when bar diameter is large and/or the concrete cover is small. Pull-out failure is caused by shearing off the concrete keys between the ribs of the reinforcement bars. That usually happens when the concrete cover is thick and/or the transverse reinforcement is sufficient. Splitting failure is weaker than the pull-out failure, see Sæther (2011).
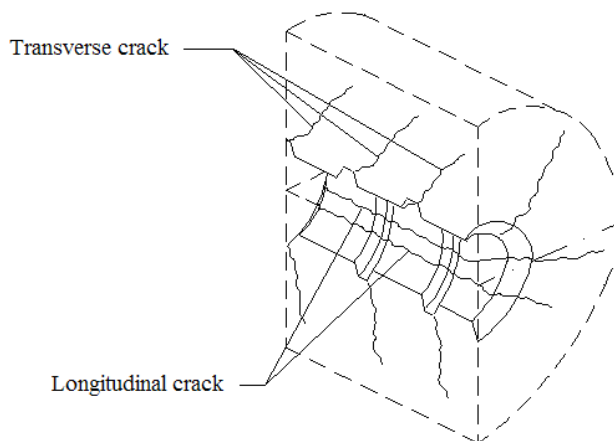
Figure 2.2   Longitudinal and transverse cracks caused by bond, modified from FIB (2000) by Berg and Johansson (2011).

2.2   Effect of corrosion

There are other factors than stress that can influence the bond between the reinforcement bars and the concrete. One of those is corrosion which is one of the most common causes of deterioration of reinforced concrete structures. Chemical reactions in the concrete form a protective layer on the metal surface. When that layer is broken down by loss of alkalinity, by carbonation of the concrete or chloride ions,

the steel becomes vulnerable to corrosion, see Domone and Illston (2010). There are two types of corrosion, general corrosion and localized corrosion. General corrosion is when the corrosion is evenly distributed along the bar length and localized corrosion is when the corrosion takes place locally and forms pits. General corrosion can be caused by either carbonation or chloride ions but local corrosion is caused by chloride ions, see FIB (2000).
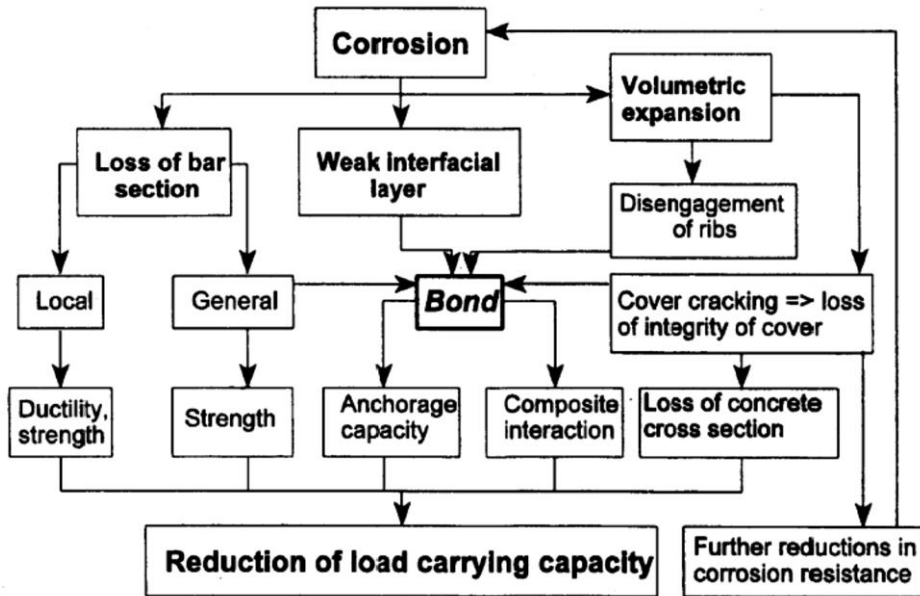
Figure 2.3   Effects of Corrosion on residual strength, from FIB (2000).

Corrosion of the reinforcements leads to loss of cross sectional area of the reinforcement bars, weak interface layer, and volumetric expansion; this is demonstrated in figure 2.3. The latter two affect the bond between the bar and surrounding concrete; tests have shown that the loss of bond is potentially much more severe than loss of cross section, see FIB (2000). The anchorage capacity of the structural member is threatened more by general corrosion rather than localized corrosion, see FIB (2000). Localized corrosion produces ions that have lower volume per unit mass than general corrosion and therefore, cracking is less likely to be caused from localized corrosion, see Val *et al.* (1998). Because the rust products occupy more volume than steel, corrosion can lead to cracking, spalling or even delamination of the concrete, see Figure 2.4.
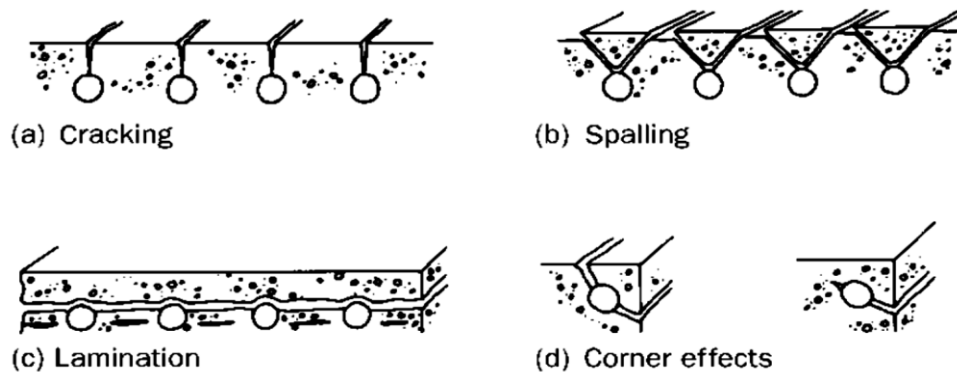
Figure 2.4   Different forms of damage from steel reinforcement corrosion, from Browne (1985).

Many factors influence the reduction of bond strength for corroded ribbed reinforcement. Those factors are among others: level of corrosion, cracking of concrete, transverse reinforcement, size and position of the reinforcement bars and size of the concrete cover. Presence of transverse reinforcement is considered to be the most important one. Lundgren (2007) suggested a classification system in order to systematically organize the effect of corrosion on the bond between concrete and the steel. Here that system is used.

When no transverse reinforcement is present bond strength is very sensitive to corrosion. Large diameter reinforcement with small concrete cover shows reduction in the maximum bond stress for small corrosion levels. Small diameter reinforcement with large cover show increase in the maximum bond stress for low level of corrosion and then drastic decrease in the maximum bond stress for higher levels of corrosion, see Lundgren (2007).

If transverse reinforcement is present, the bond is much less sensitive to corrosion. For large diameter bars with small covers the maximum bond stress is almost constant from no corrosion to higher level of corrosion. However for smaller diameter bars with larger cover there is an increase in the maximum bond strength for low levels of corrosion. For higher levels of corrosion the maximum bond strength decreases to a level similar to what it was for uncorroded, see Lundgren (2007).

Most research on corrosion in reinforced concrete has been done with artificially corroded specimens. In order to accelerate the corrosion, electric current is applied to the reinforcement. Researches show that specimens subjected to low current density had lower bond strength than those subjected to high current densities. Therefore, it is natural to assume that it is hard to achieve a satisfactory correlation between artificially produced corrosion and natural corrosion. The large increase in bond strength at high levels can be explained by accelerated test conditions. For naturally corroded reinforcement where the corrosion takes a long time, the rust might be more easily dissolved through the concrete cover, resulting in less built up radial stress than for artificially corroded reinforcement, and therefore less increase in bond strength for corrosion of low level, see Sæther (2011).

3 Test programme

The specimens were collected from north side of Stallbackabron in Trollhättan in November and December 2011. They were transferred to Chalmers University of Technology in February 2012 and tested in April and May 2012.

Figure 3.1   Stallbackabron in Trollhättan, from www.svevia.se.

3.1 Test specimens

The test specimens are originated from Stallbackabron in Västra Götaland, the bridge is part of road E45 and road 44 and crosses the Göte Älv River in Trollhättan. It is a link between Stallbacka industry area and Överby shopping centre and is the most important link between Trollhättan and Vänersborg. The bridge has been in service since 1981. In 2010 it was recorded that each day 30,000 vehicles travel across the bridge. The bridge is one of the largest bridges in Sweden, 1.392 meters long. It has a navigable height of 26 m and four lanes, total width of 14.95 m. It is a composite bridge the deck is made of reinforced concrete resting on steel beams. A cross section of the bridge deck can be seen in Figure 3.2.
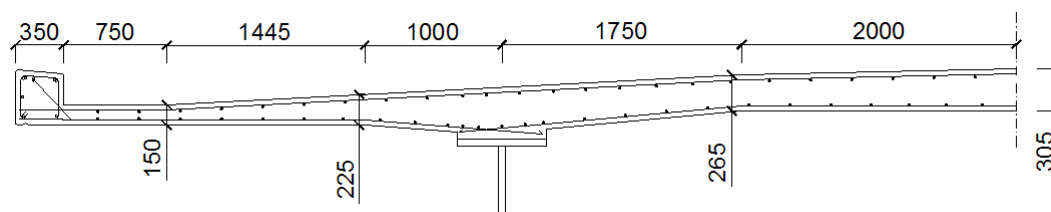
Figure 3.2 Section cut of the bridge deck.

Even though it had only been in service for 30 years extensive rehabilitations were needed. The reason for that is mainly poor design of the bridge. Edge beams were carrying more load than they were designed for and subsequently they cracked because of that. Another factor is that the steel railing was cast into the concrete and causes stresses in the edge beam. It was noticed that transverse cracks initiated at the

railing sometimes were all across the cross-section. After cracking is initiated corrosion is more rapid because it is easier for the de-icing salts to penetrate trough the concrete to the reinforcement. De-icing salts are considered to be the one of the biggest cause of corrosion of steel in concrete; however research has shown that using de-icing salt is still more economical than using the other alternatives, see Broomfield (1997). In order to extend the service life of the bridge, there was a need to replace the edge beams and the outermost part of the slab. The edge beams were suitable for this research since they are naturally corroded and have different extent of damage, from no damage to corner spalling. In Figure 3.3 part of an edge beam can be seen.

Figure 3.3   Edge beams and part of the slab after being sawn from the bridge.

Stirrups are made of Ks40 and are of diameter 10 mm and with spacing of 300 mm. Longitudinal reinforcement is made of Ks60 and is of diameter 16 mm. In the bottom is one bar in each corner and in the top there are two bars bundled in each corner. There is also one longitudinal bar on the outside edge of the beam. The guarding rail is cast into the concrete with additional reinforcement around those rails, as can be seen in *Figure 3.4*.
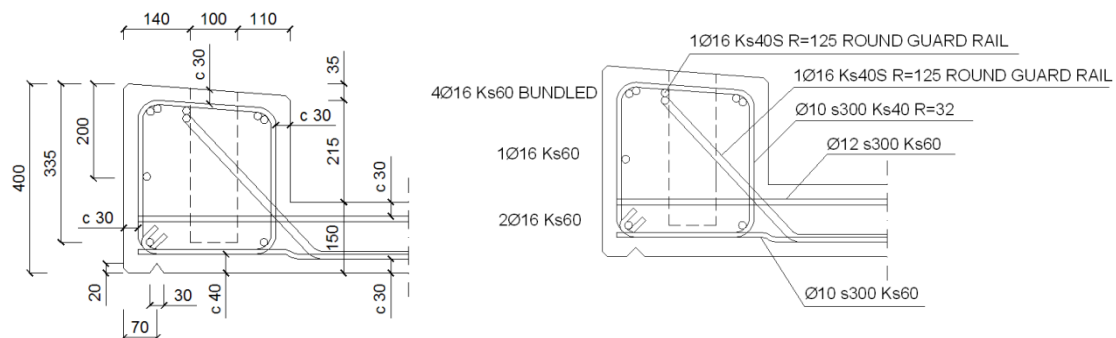
Figure 3.4   Section cut of the edge beams.

Tests on 8 specimens from the southern part of the bridge were tested by M. Tahershamsi (2012). In this thesis specimens from the northern part of the bridge were tested. Initially it was planned to test 15 specimens but due to problems with measuring device, testing was delayed for five weeks. Therefore, it was not possible to test all the specimens within this thesis project; 10 specimens were prepared but only five were tested. Berg and Johansson established a classification system that Tahershamsi began to use. In that system, the beams were classified based on how much damage they had. There were five classes. That system turned out to be too complicated in practice so a new system was established and is used in this thesis. That system consists of 3 damage classes: reference, without any visible cracking; medium damage where the specimens were cracked but did not have any spalling; and finally a high damage where the specimens showed both cracking and spalling of the concrete cover, see Figure 3.5. The beams were named with a letter according to damage class and a number, for example M5, a medium damaged specimen number five. That is the same naming system used earlier by Berg and Johansson, and Tahershamsi in 2011 and explains why we start with number M4. The five specimens tested in this round were randomly taken from a group of 15 specimens which explains the non-consecutive naming.
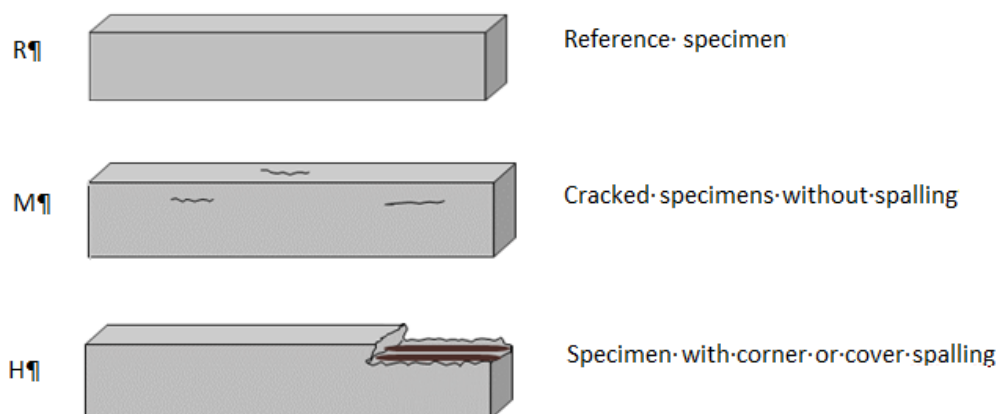
Figure 3.5   Classification for damage of test specimens.

When working with the specimens deviations from drawings were noticed. Concrete cover was not accurate and there was reinforcement bars in the beam that were not on the drawings. The bars were also spliced; therefore in some of the beams at certain locations there was one extra bar. Deviations of the concrete cover can be seen in Table 3.1 for both ends of each test specimen. Notations are found in Figure 3.6.
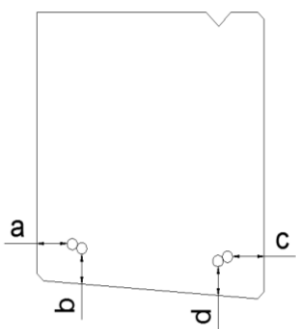
Figure 3.6   Notations for concrete cover.

The concrete cover was designed to be 30 mm on the top and the sides of the beam but 40 mm at the bottom. The real concrete cover to the main bars varied a lot from that, from 40 mm to 75 mm.

Table 3.1   Measured concrete cover.

	South end				North end			
	a [mm]	b [mm]	c [mm]	d [mm]	a [mm]	b [mm]	c [mm]	d [mm]
R6	50	40	65	50	55	55	60	45
M4	70	50	40	65	30	65	70	45
M5	65	45	55	65	55	65	55	50
M6	45	60	45	70	35	50	65	35
M7	75	55	35	65	30	75	65	50
M9	45	50	55	50	55	55	45	50
M11	60	70	35	65	50	50	80	55
M12	60	50	40	60	35	85	60	60
H5	70	30	65	55	50	50	60	30
H6	70	55	30	60	35	70	60	55

Very little damage was on the bottom side of the beams; mainly all damage was on the upper surface. That is reasonable because the top side has been exposed to de-icing salts but the bottom side was sheltered. In a previous master thesis it was decided to turn the beams upside down in the test set up, see Berg and Johansson (2010). Another advantage with turning them is that then the load is applied to a flat surface instead of an inclined surface.

In order to repair the bridge the edge beams and part of the bridge deck were sawn off and replaced. Before sawing the specimens off the bridge they were chosen and documented; 30 specimens from the north side off the bridge were chosen, cracks marked and crack widths were measured and documented. The edge beams and part of the slab was cut off in elements of 3-4 m, see figure 3.3. The elements were transferred to a nearby storage site where they were stored. 15 of them were chosen to be tested. The slab was sawn off and they were sawn into correct length. It was important to have at least one stirrup between the end of the beam and the support and therefore it was important that the specimens were cut in right places. Specimens were transferred to Chalmers University of Technology where they were further prepared and tested. During transfer and sawing, specimens M4 and M6 got damaged so they went from medium to high. After the transfer they both had spalling on one end and it is considered to be caused by both transvers cracks from the corroded reinforcement that opened more and because of careless handle while sawn to correct length.

3.2 Test setup

Detailed design of the test set up and strengthening of the beams were needed in order to secure that bond slip failure would occur. Test set up and strengthening designed by Berg and Johansson was used. A four point bending test indirectly supported was used, as can be seen in figure 3.7. Directly supported test setup could not be used since the support pressure would improve the bond of the reinforcement over the support.
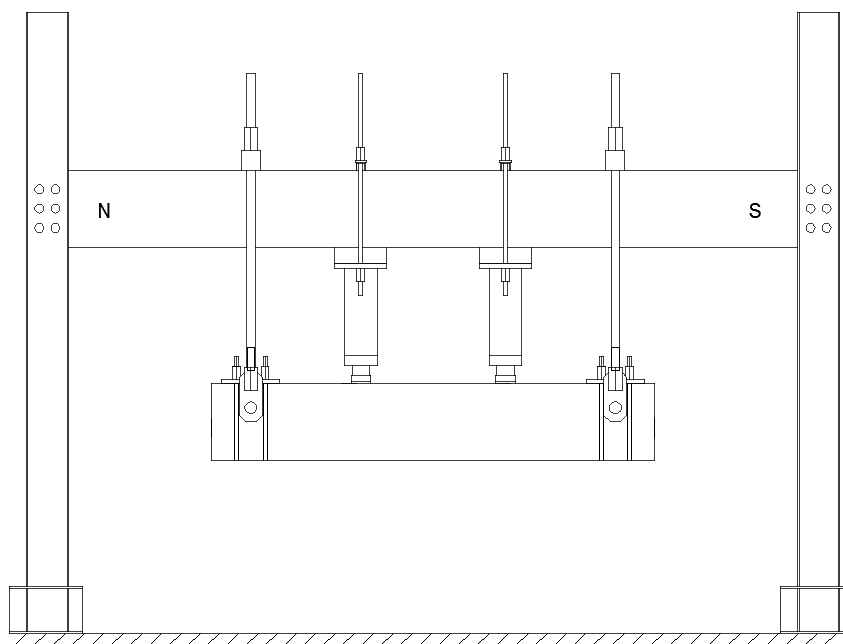
Figure 3.7   Test set up.

Anchorage resistance of indirectly supported beam is lower than for directly supported beam. To be able to get bond failure the beam needed to be strengthened in order to transfer the shear force up to the support. That was done with four ø20 mm fully thread reinforcing bars of high yield steel glued to the concrete with epoxy and anchored at the top with a steel plate and four hexagonal nuts at each end. The epoxy

used came from Nils Malmgren AB. It is a two component material, injection *NM Injektering INP 32* and hardener *NM Härdare 24 L.* According to the manufacturer, the tensile strength of the component is 20 MPa and the adhesion to the concrete is 3.5 MPa.
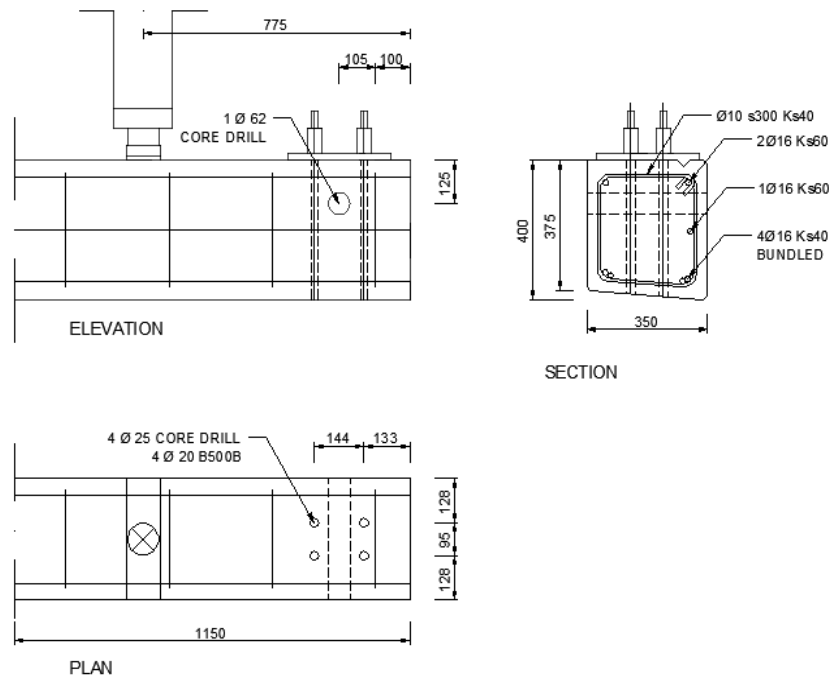
Figure 3.8   Load arrangement, placement of the support and the strengthening bars.

Before drilling the specimens, the end stirrup had to be carefully located using a detector Profometer 3 – rebar locator. Next, the position of the support hole was marked, and finally, the position of the strengthening was marked. In few cases it was necessary to move the support hole closer to the centre in order not to drill through the stirrup. In those cases the support hole on both sides was moved closer to the centre in order to keep symmetry, see Figure 3.9 and table 3.2 for variations between specimens.
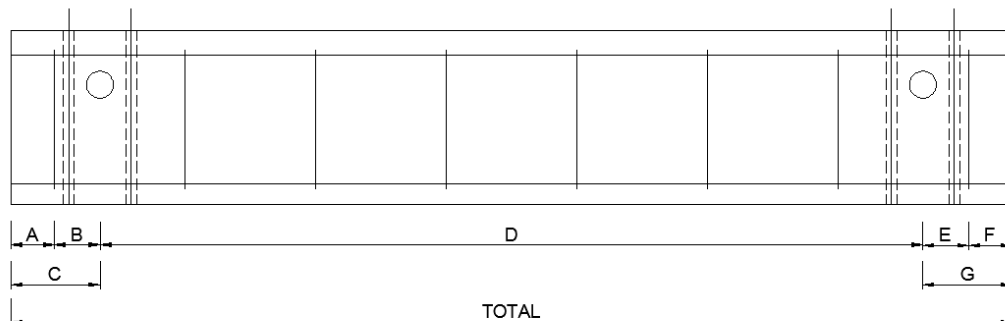
Figure 3.9 Position of the support holes.

Table 3.2   Measurements of the test specimens, see measurements in Figure 3.9.

	A [mm]	B [mm]	C [mm]	D [mm]	E [mm]	F [mm]	G [mm]	TOTAL [mm]
R6	140	110	250	1815	185	65	250	2315
M4	105	100	205	1875	165	40	250	2285
M5	139	86	225	1882	129	96	225	2332
M6	75	130	205	1895	150	55	205	2305
M7	110	95	205	1893	120	85	205	2303
M9	85	120	205	1878	110	95	205	2288
M11	100	95	195	1886	85	110	195	2176
M12	110	95	205	1885	110	95	205	2295
H5	80	125	205	1890	115	90	205	2300
H6	130	110	240	1800	190	50	240	2280

The support hole had a diameter of 62.0 mm and the steel bar used for support had a diameter of 61.2 mm. Therefore it was very important when drilling the holes that they were straight so there wouldn't be any problems getting the steel bar through the hole. Holes for the strengthening bars were with diameter of 25 mm and the strengthening bars were with diameter 20 mm. All the holes were drilled with an electric driven water cooled core drill, with diamond tipped core drill.

Before testing the specimens were documented. All visible cracks were marked and crack widths were measured and compared to old measurements if they existed, see Appendix E and Appendix F. The crack widths were from 0.1 mm to 3.2 mm The specimens were thoroughly photographed from various angles, to keep the former look of the beams documented, see examples in Figure 3.10 and Figure 3.11 (both from beam M6).

Figure 3.10   Example of documentation of specimen.

Figure 3.11   Example of pictures for documentation of specimen.

Before each test a number of LVTD:s were connected to the beam, 4-5 on each short side, 15 on the top, 8 on the bottom and 3 lateral. The LVTD:s measured the displacements during loading. The position of the LVTD:s for beam M5 is shown in Figure 3.12. The LVTD:s on the short sides measured free end slip of the main bars. Those LVTD:s are put on a steel plate which is drilled to the concrete. The mid of the plate is 185 mm from the top of the beam. The LVTD:s on the bottom measured free end slip of the strengthening bars. Those are connected the same way as the short end LVTD:s, the mid of the plate is 275 mm from the support. The LVTD:s on the top measured mid span deflection, deflection close to the load, and support settlements, both on the concrete and on the steel hanger. Those LVDT's are fastened to stands on the floor. When testing M5 all LVTD:s on the short sides measured displacement of the reinforcement. Next, when testing specimen M9, a LVTD number 33 was added and that and LVTD number 19 mesured the displacement of the concrete on each short end. When testing the last three specimens 4 LVTD:s were moved to mesure the displacement of the concrete close to the bottom of the strengthening bars, see Figure 3.12.
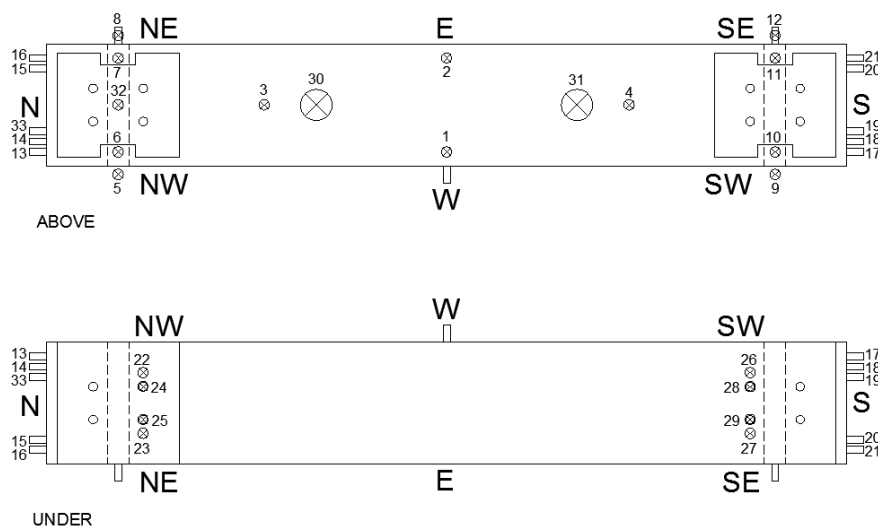

Figure 3.12   Numbering of LVTD:S on the top and bottom of R6, M4 and M6.

3.3 Material properties

3.3.1 Concrete

In previous master thesis by Berg and Johansson (2011), a compressive strength of 38 MPa was used for the 2D non-linear analysis and the fracture energy, tensile strength and Young's modulus were calculated from the compressive strength.

When the two first beams were tested, in earlier thesis, a series of five cylindrical compressive strength tests were done according to the Swedish Standard SS-EN 12390-3. The test specimens were drilled and cores had a height of 108 mm and a diameter of 54 mm. The specimens were drilled according to Swedish Standard SS-EN 12504-1. The mean value from five tests gave a compressive strength of 49.5 MPa, see Berg and Johansson (2011)

To ensure that the cylindrical compressive strength tests gave reasonable values the compressive strength was also measured with a series of ten tests with test hammer. The test hammer, type N, had impact energy of 2,207 Nm. The test was carried out on the short side of the beam. Those tests gave a mean value of 44.0 MPa, see Berg and Johansson (2011).

The FE analysis in this study was compared to experimental work ; therefore it was important to have the behaviour as accurate as possible. In order to achieve that, mean values are used for the non-linear analysis. Because of variations of the compressive strength in the two tests the mean compressive strength was probably somewhere in between and for the analysis it was chosen to use a value of 48 MPa, see Table 3.3. Using that value was later verified by comparing the model results with the experiments.

Table 3.3 Material parameter of concrete.

	f_{cm} [MPa]	f_{ctm} [MPa]	E_{cm} [GPa]	G_f [N/mm]
Concrete	48	3.5	35	0.147

The tensile strength of the concrete was calculated from compressive strength according to the equation below, given in FIB (2010).

$$f_{ctm} = 0.3 \cdot f_{ck}^{\frac{2}{3}} \ for \ concrete \ grades \ \leq C50 \tag{1}$$

The calculated tensile strength was 3.5 MPa. For frost damaged concrete, it has been shown that the tensile stress is more affected by the frost damaged than the compressive resistance, see Hanjari (2010), who suggested an equation to calculate the tensile strength of frost damaged concrete, see below. Even if the specimens didn't have any visible signs of frost damage, it can be argued that they had been exposed to frost and the corrosion damaged concrete might also follow the same behaviour to some extent.

$$f_{ctm} = 0.027 \cdot (f_{cc}^{d})^{1.2} \tag{2}$$

When this expression was used, the tensile strength was 2.67 MPa. This gave reason to run analysis with lower tensile strength to correspond better to the experimental results if needed, see chapter 4.3.

The fracture energy is defined as the energy per unit area which is required to break bonds in a fracture process. It is recommended to determine the fracture energy from tests but in the absence of experimental data the fracture energy can be calculated from FIB (2010) as:

$$G_f = 73 \cdot (f_{cm})^{0.18} \qquad (3)$$

The fracture energy of normal weight concrete depends mainly on the water-cement ratio, the maximum aggregate size and the age of the concrete. Other factors such as: size of the structural member and curing conditions also play a role. In the model code from 1990 the fracture energy was not only determined by the compressive strength but also from the size of the aggregates, see FIB (1993). However aggregate type and the shape seem to influence the fracture energy much more than the aggregate size, see FIB (2010).

Calculated fracture energy for the concrete with mean compressive strength of 48 MPa was 0.147 N/mm. However, from Figure 3.13 it can be seen that the fracture energy varies from 0.10 N/mm to 0.19 N/mm. Since no reliable data regarding the aggregate's specifications of the constructed bridge, could be found, mean value was used, see Table 3.3. This also gave reasons to run analysis with different fracture energy values in order to get better correlation between the experiments and the FE analysis, see 4.3.
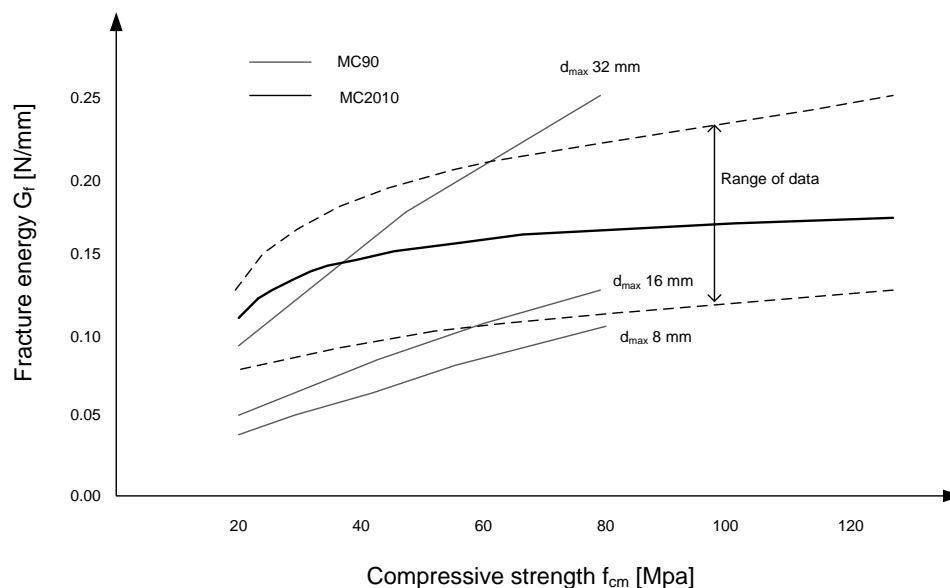
Figure 3.13   Comparison of fracture energy between Model code 1990 and model code 2010, modified from Müller (2009).

3.3.2   Steel reinforcement

No tests were done on the steel reinforcement for this thesis. Previous testing on same kind of steel reinforcement had been conducted at Chalmers University of Technology, see Appendix A. Those values were used in the non-linear 2D modelling. High yield pre-stressing steel from Dywidags was used for strengthening around the hole and values received from the manufacturer, see Table 3.4. It was later found out that the steel reinforcement never reached yielding. Therefore, it is only Young's modulus that affects the behaviour, see chapter 4.4.

Table 3.4 Material parameters for reinforcement steel

	f_{sy} [MPa]	f_{su} [MPa]	ε_{sy} [%$_0$]	ε_{su} [%$_0$]	Es [GPa]
KS60	693	907	0.312	1.25	222
KS40	468	638	0.227	1.14	206
Strenghtening	500	550	0.243	1.05	205

3.4 Results

As can be seen in Figure 3.14 all the specimens had similar behavior up to the failure load. However, the maximum load is quite different for the specimen; it varied from 178 kN to 316 kN. The specimens were first loaded up to 35 kN and then unloaded. Then they are loaded to their maximum capacites. At a load level of approximately 75 kN the loading was stopped and all the visible surface cracks were marked if. This was done in intervals of every 10 kN after the load level of 75 kN; which explains the disrupts which can be seen in Figure 3.14 where the load is plotted versus the mid span deflection. The load is average of the two point loads, and the mid span deflection is taken as the average of the measurements of the two LVDT:s in the mid span, corrected for the deformations of the supports, measured on top of the specimen.
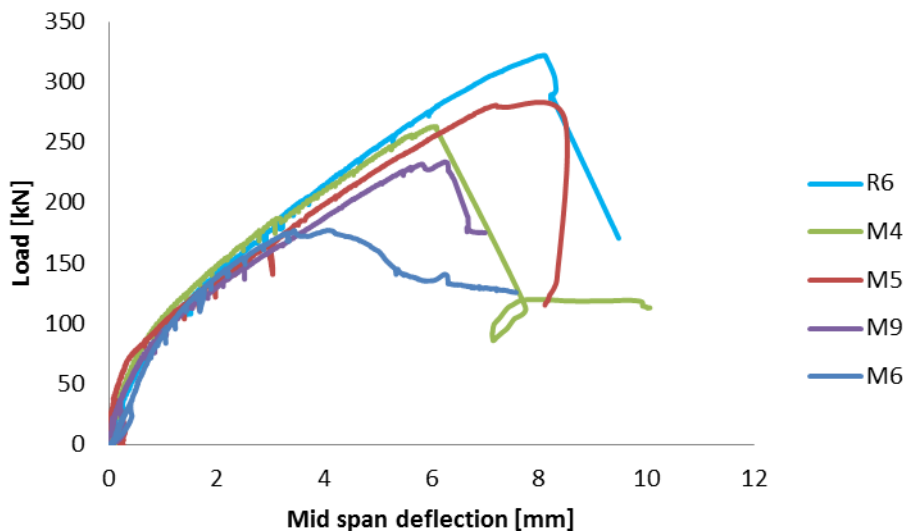
Figure 3.14 Average load as function of mid span deflection for the test specimens.

First flexural cracks were observed at load levels of 85 – 115 kN, they were usually located close to the load within the shear span of the beam. Due to safety issues a safety stand was put on each side of the mid span in order to avoid injuries if the beam would twist in the test set up. Those safety poles made it hard to observe if there were any cracks in the mid span. As the load was increasing cracks propagated. Shear cracks started at the load levels of 130 to 175 kN; usually the first shear crack started around 500 mm from the end of the specimen. In the tests the free end slip of the strengthening bars was measured for lower load than the free end slip of the main

CHALMERS, *Civil and Environmental Engineering,* Master's Thesis 2012:80

reinforcement but usually smaller slip was observed than for the main reinforcement. After the main reinforcement start to slip a splitting crack forms along the bar in some cases booth on the side and on the bottom of the specimen, see Figure 3.22.

Figure 3.15 Final crack pattern of west side of beam M5.

As can be seen in Figure 3.15 and Figure 3.16, after the shear crack was initiated, the crack propagated upwards and later another shear crack started closer to the support. That crack propagates further upwards and in some cases it intersected the earlier shear crack. When free end slip of the strengthening bars was measured
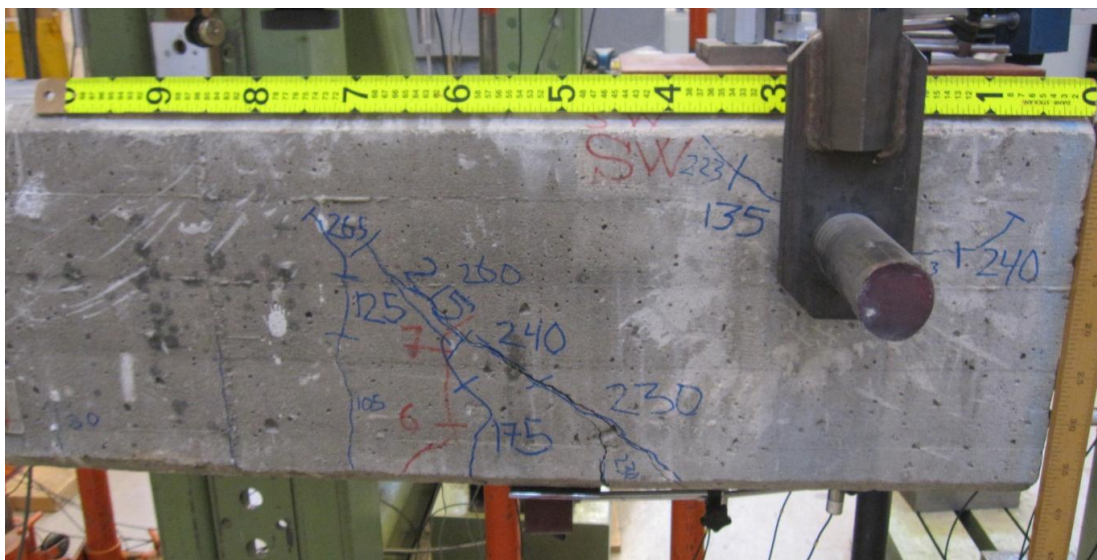
Figure 3.16 Final crack pattern of the failure end on the SW side of the specimen M5.

Table 3.5 Test results, explanations for notations regarding sides can be seen in Figure 3.12.

	Max. load [kN]	Max. deflection [mm]	Load when measureable free end slip started [kN]	Available anchorage length [mm] and side	Max. load / average available anchorage length [kN/mm]
M4	263	6.08	255	420 SE 430 SW	0.62
M5	281	7.20	255	430 SE 430 SW	0.65
M9	234	6.25	226	270 SE 400 SW	0.70
R6	322	8.31	307	430 NE 440 NW	0.74
M6	178	4,1	170	300 SE 90 SW	0.91

Table 3.6 Load level for cracking.

Side	First shear crack [kN]					First flexural crack [kN]				
	M4	M5	M9	R6	M6	M4	M5	M9	R6	M6
SE	155	145	173	205	135	115	105	165	85	135
SW	185	175	225	160	155	-	95	92	-	155
NE	175	-	173	185	-	-	-	-	185	-
NW	155	140	120	170	-	-	-	-	170	-

The available anchorage length was defined as the length from the end of the specimen to the shear crack closest to the support at the height of the main reinforcement, see Figure 3.17. It varied from 90 mm to 430 mm. Specimen M5 and R6 had the support hole closer to the mid span than specimens M4, M6 and M9, which can possibly to some extent explain why M5 had higher ultimate load than the other medium specimens. The available anchorage length for the specimen M6 was much shorter than for the other specimens, that was explained by the early slip of the strengthening bars see Figure 3.24. Even though available anchorage length became much shorter for specimen M6 than the other it got higher load capacity related to the available anchorage length, ratio between the maximum load and the average

available anchorage length was 0.91 for M6 compared to 0.62-0.74 for the other specimens, see Table 3.5.
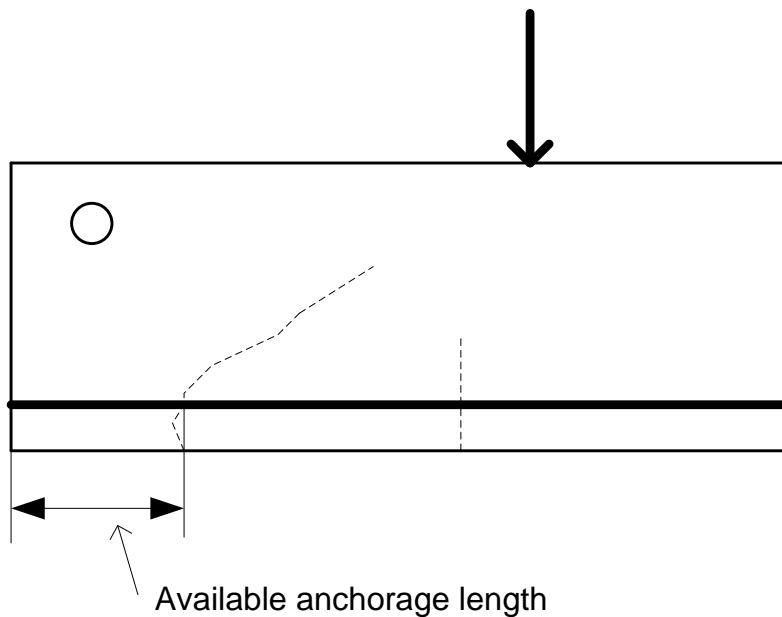
Figure 3.17 Explanation of the available anchorage length.

On Figure 3.19 the displacement for the bottom reinforcement for specimen M5 has been shown, it can be seen that a negative slip was measured in the tests. These values were not free end slip but caused by deformation of the beam's end section under loading. That was later verified by having one LVTD on each end of the beam measuring the displacement of the concrete and the other four LVDT:s were measuring the displacement of the reinforcement, see Figure 3.18.
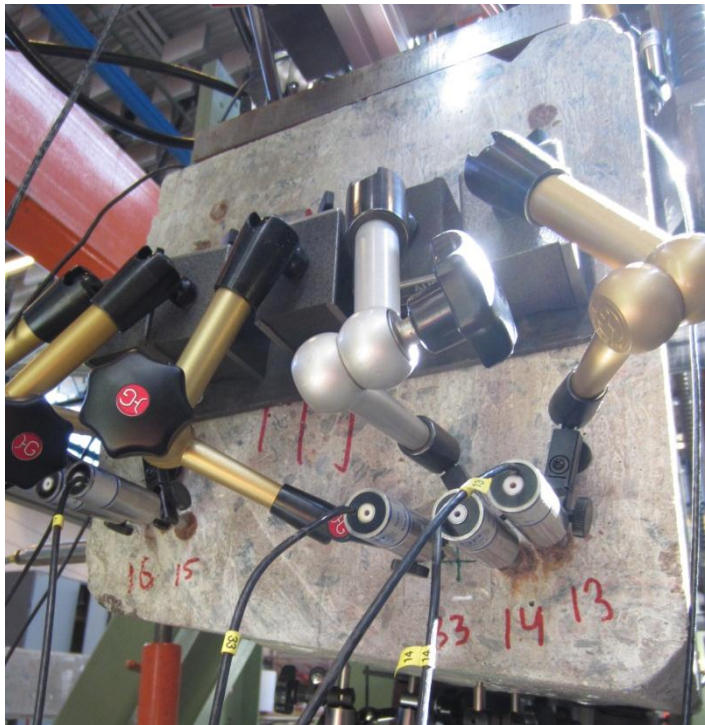
Figure 3.18   LVDT:s on short side of specimens.
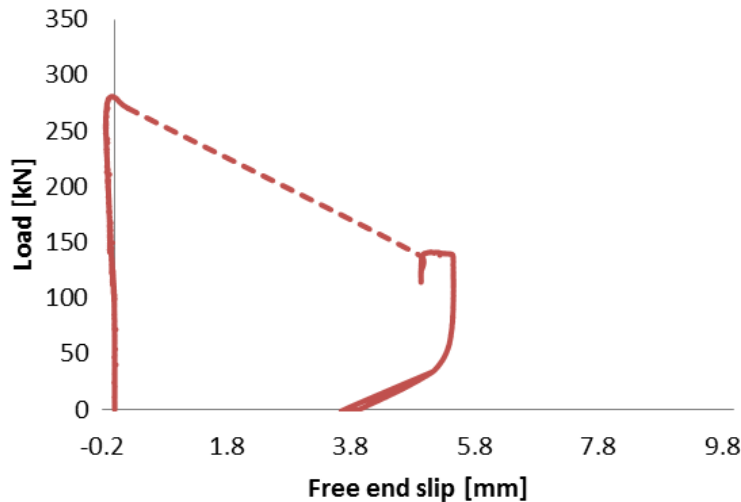
Figure 3.19 Displacement of main reinforcement in test specimen M5.

The difference of the displacement of the concrete and the reinforcement can be seen in Figure 3.20. Behavior of the free end slip in the early stages can be seen in Figure 3.21. Those values should be considered carefully since placement of the LVTD on the concrete was not in line with all the main reinforcement bars. Measurable free end slip started for a load between 170 and 307 kN which was 90 to 97 % of the maximum load and the final anchorage failure occurred at the moment of maximum load. However load level of 80 to 140 kN very small free end slips were seen in the analysis less than 0,01 mm, those values are not considered measureable. When the bar started to slip, a crack formed along the bar either on the bottom or on the side, see Figure 3.22. The LVDT:s gave one measurement every second, in Figure 3.19 and Figure 3.20 the dotted line represents only one measurements. From that it can be seen that the failure for specimens M4, M5 and R6 was more abrupt than the failure of specimens M6 and M9.
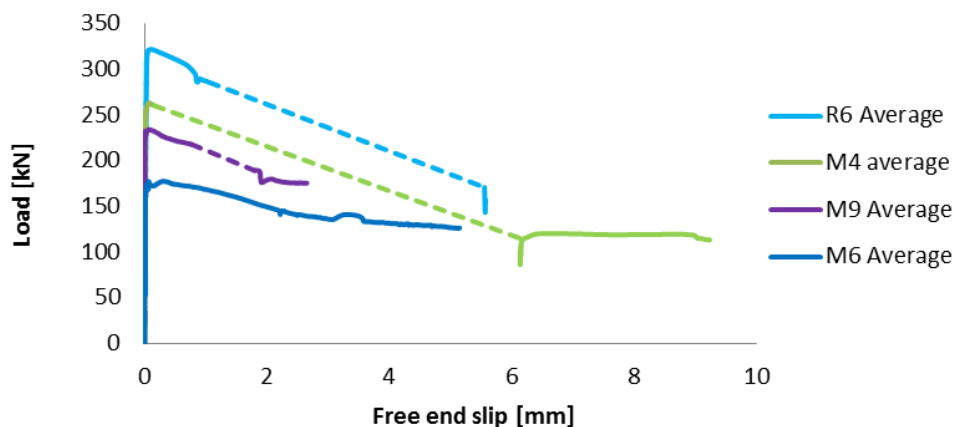
Figure 3.20 Free end slip of main reinforcement, dashed line represents were the measurements are not continuous.
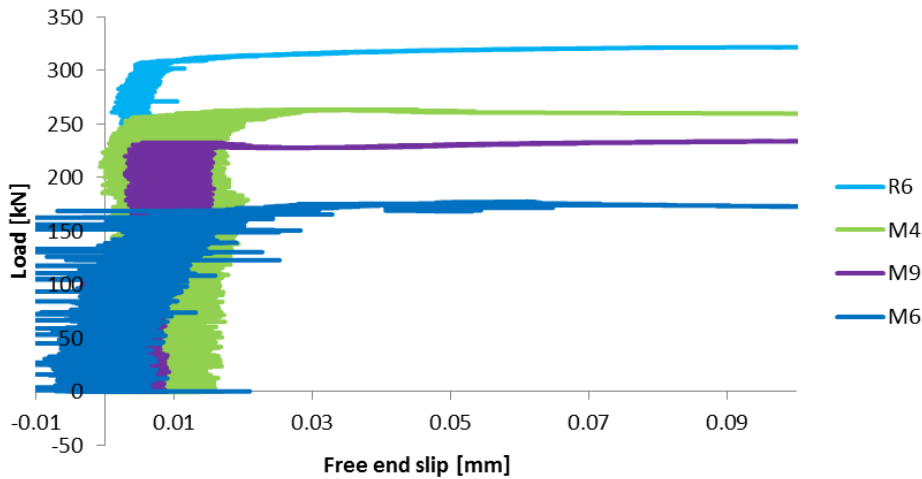
Figure 3.21 Enlarged free end slip of main reinforcement.
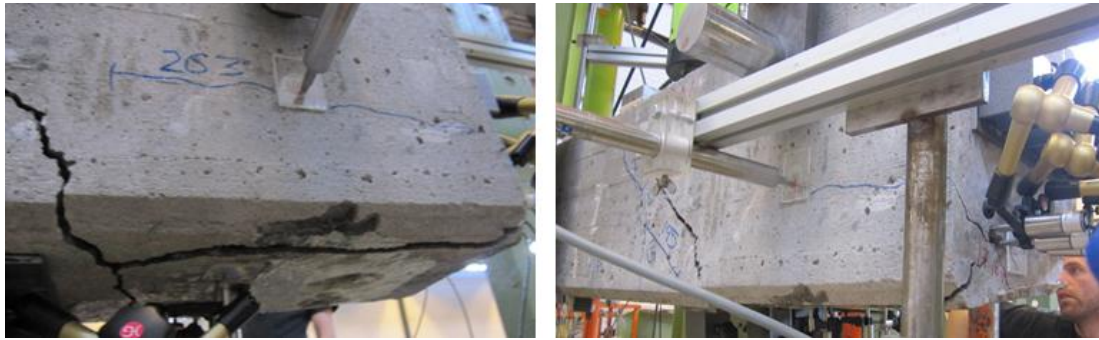
Figure 3.22 Crack along reinforcement on beam M4.

In all the specimens, the behavior of the free end slip was similar except for specimen M6. That was explained by slip of the strengthening bars and is discussed more in detail in the following paragraph. For specimen M9 the free end slip was less than what was seen for the other specimens. That can be explained by the fact that the available anchorage length was shorter for specimen M9 than for the others, mean available anchorage length was 335 mm compared to around 430 mm for the other specimens.

After two tests it was decided to change the setup of LVDT:s so that it became possible to measure free end slip of the strengthening bars, see arrangement in Figure 3.12. In Figure 3.23 and Figure 3.24 free end slip of the strengthening bars can be seen. Slip of the strengthening bars were observed before ultimate load was reached, the magnitude of the slip for specimens R6 and M4 are very small compared to the free end slip of the main reinforcement. For specimen M4 it is clear that the strengthening bar on SE side started to slip faster at a load level of 150 kN and slips till a load level of 225 kN is reached, then SW side started to slip faster and the force is transferred to the SW bar and the free end slip of the strengthening bar on the SE side decreases.
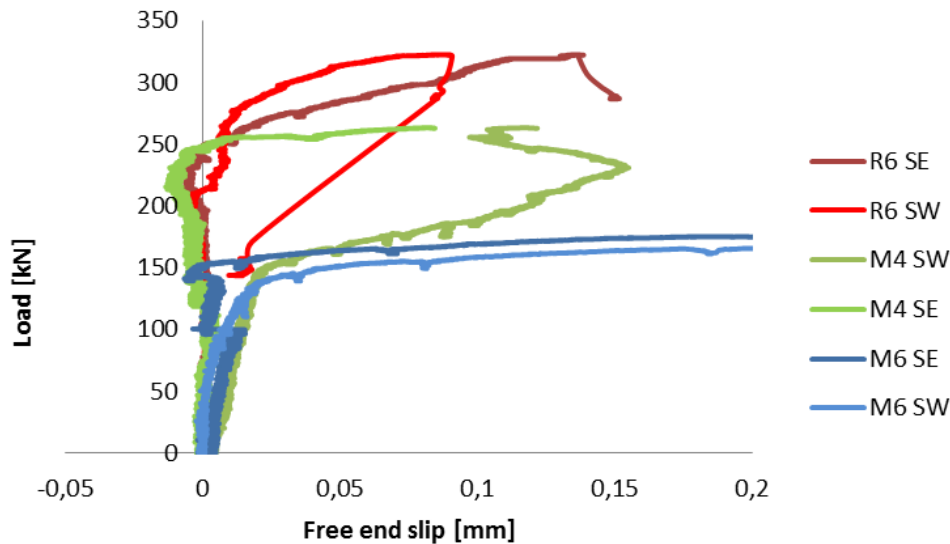
Figure 3.23 Enlarged free end slip of strengthening bars.
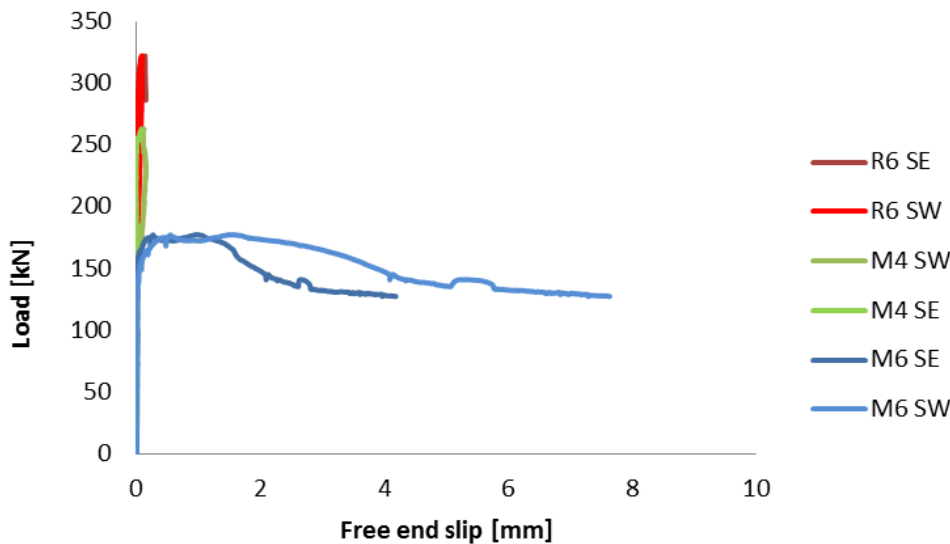
Figure 3.24 Free end slip of strengthening bars.

By looking at the free end slip of the strengthening bars in Figure 3.24 it can be seen that strengthening bars in specimen M6 slipped. On the south west side slip started before maximum load was reached then the strengthening bar on the south east side began to slip. That explains why it had so much lower resistance than the other specimens. Furthermore it gives reason to exclude it from comparison with the other ones since it had another failure mechanism than the other. By inspecting the specimen, it was noticed that the bond between the epoxy and the concrete failed. Not a good explanations was found about why specimen M6 had worse epoxy bonding between –strengthening bars and the concrete than the other tested specimen, as stated earlier it started to slip on the south west side and that side had no visual cracks while the south east side had.

If test specimen M6 is excluded from the comparison because of the bond failure of the strengthening bars, it can be seen that the ratio between the force and mean available anchorage length is 0.62-0.74.

CHALMERS, *Civil and Environmental Engineering*, Master's Thesis 2012:80

4 FE analysis

4.1 FE model

A 2D model was modified from Berg and Johansson (2010). Only half of the beam was modelled with symmetry line on one edge, see Figure 4.1. Non-linear FE analysis based on non-linear fracture mechanics was carried out. The model was created using Midas FX+ version 3.0.0 post- and pre-processor. Results were also analysed in Midas FX+. All the analyses were run by using Diana Version 9.3.0 on a cluster; this was mainly because it was easier to run a phased analysis on a cluster than on Windows. It was also beneficial with regard to the calculation time. All the material data had non-linear response; the material data can be seen in the data file in Appendix B. The model consisted of about 5300 elements and element size was 10 mm. Execution time was around 30 minutes.
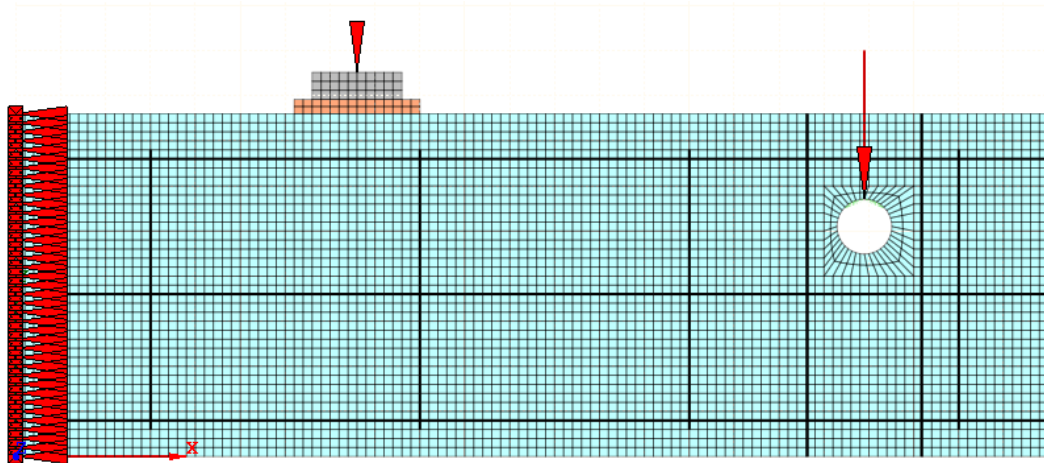
Figure 4.1 Picture of the FE model.

The concrete was modelled using quadrilateral plane stress 4 node elements Q8MEM, see DIANA (2008). The compression response of the concrete was described by the expression of Thorenfeldt, see THOREN in DIANA (2008). The tension softening was described by the expression of Hordijk, see HORDYK in DIANA (2008). A rotating crack model based on total strain was used for the concrete. Cracking of the concrete was modelled with smeared crack approach and the crack band width was chosen equal to the element size, corresponding to an assumption that cracks are localized in single element rows. This assumption was later verified to be correct in contour plots of the strain, see Figure 4.8. Chosen input parameters are discussed in section 3.3.

There were three different types of reinforcement in the model: strengthening bars of high yield ribbed steel and two types of reinforcement, KS60 and KS40, see Figure 3.8. Behaviour of all the reinforcement was modelled with Von Mises yield criteria, material parameters for the reinforcement can be seen in Table 3.4. The top bars and the stirrups were modelled as embedded reinforcement in the plane stress elements, which means that they add stiffness to the model. They don't have degrees of freedom of their own thus, perfect bond between the reinforcement and the surrounding concrete was assumed. The bottom bars, the mid bar and the strengthening bars around the support were all modelled with truss elements, including the bond-slip model in interface elements. This bond model is further explained in chapter 4.2.

The model had one support and a symmetry line, see Figure 4.1. At the symmetry line translations in all nodes were restricted into the plane and along the beam; the nodes were only free to move up and down. The support was modelled as a circular hole through the concrete plane stress elements. A dummy suspension was modelled in order to provide a wider support. It was modelled as an L6BEN 2 node 2D class-I beam element, see L6BEN in Diana (2008). The lower node, see Figure 4.2, called master node, was tied to 10 nodes on the edge of the hole, called slave nodes, to create more stable support. The nodes were connected with eccentric connection; see ECCENT in Diana (2008). This means that the relative distances between the nodes were kept constant but the group was allowed to rotate. The hole, dummy suspension and the links between the master node and the slave nodes can be seen in Figure 4.2. The top node of the two strengthening lines and concrete were tied together with equality connection that makes the displacements of the nodes equal, see EQUAL in Diana (2008). That was done because in reality the strengthening bars were anchored at the top with a steel plate and hexagonal nuts.
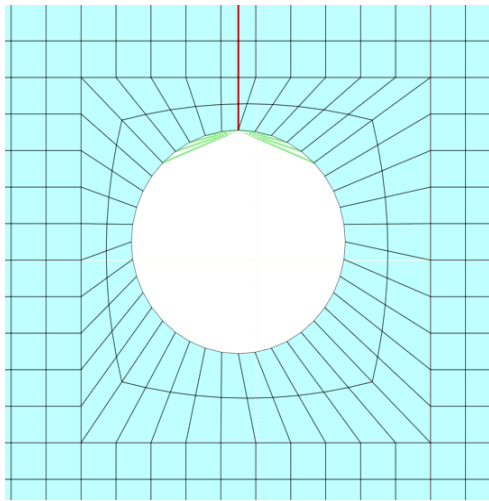
Figure 4.2 The hole, dummy beam and eccentric connections between nodes.

In reality, the load was applied on a steel plate and between the steel plate and the concrete beam there was a fibre board plate. Those were also modelled in the analysis. Timber and steel plate were modelled with the same elements as the concrete, four-node quadrilateral isoperimetric plane stress elements.

Loading was done in two phases. In the first phase, self-weight was applied. In the second phase, load was applied on the centre point on the steel plate. It was applied with deformation control, so the displacement of the point under the load was 0.05 mm in each step.

4.2   Bond of reinforcement

The bottom, the mid and the strengthening bars were modelled using L2TRU two-node, 1 D truss bar elements, see L2TRU in DIANA (2008). The interface layer between the reinforcement and the concrete was modelled with L8IF two plus two nodes, 2D element, see DIANA (2008). The interface layer connected the concrete to the steel bars. The thickness of the interface layer corresponds to the circumference of the steel bars. Circumference of two bundled bars can be described by an upper and a lower limit, see fig Figure 4.3 see Jirsa *et al.* (1995). In this case, the maximum value

was 100.5 mm and the minimum value was 82.3 mm for two bars. In this thesis an average value of the calculated maximum and the minimum was used. This value corresponds to the circumference of 3.6 bars for the four bottom bars or 125,6 mm for each of the bundles.
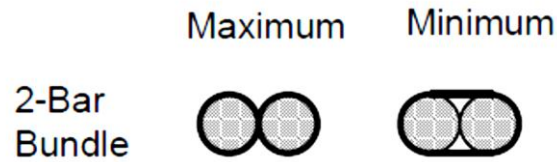
Figure 4.3 Maximum and minimum values of the circumference of two bundled bars, see Jirsa et al. (1995).

CEB-FIP 2010 model code describes how bond between the reinforcement steel and the concrete can be modelled. The values in Table 4.1 and the equations below are used to calculate the bond slip curve, see Figure 4.4. The multi-linear bond slip curve is used to model the bond slip between the reinforcement and the concrete.

$$\sigma_c = \tau_{max} \left(\frac{s}{s_1} \right)^\alpha \ for \ 0 \leq s \leq s_1 \tag{4}$$

$$\sigma_c = \tau_{max} \ for \ s_1 \leq s \leq s_2 \tag{5}$$

$$\sigma_c = \tau_{max} \left(\tau_{max} - \tau_f \right) \frac{s - s_2}{s_3 - s_2} \ for \ s_2 \leq s \leq s_3 \tag{6}$$

$$\sigma_c = \tau_f \ for \ s_3 \leq s \tag{7}$$

There are two main cases: Pull-out failure and splitting failure. Pull out failure is valid for well confined concrete; concrete cover $\geq 5\text{Ø}$ and clear spacing between bars $\geq 10\text{Ø}$. Splitting failure is valid for $\text{Ø} \leq 20$ mm and other restrictions regarding the concrete cover, see FIB (2010).

Table 4.1 Parameters for defining the mean bond stress slip relationship for ribbed bars, see FIB (2010).

	Pull-Out failure		Splitting failure			
	Good bond conditions	All other bond conditions	Good bond conditions		All other bond conditions	
			Unconfined	Stirrup	Unconfined	Stirrup
τ_{max}	$2.5\,(f_{ck})^{0.5}$	$2.5\,(f_{ck})^{0.5}$	$7.0\,(f_{ck}/20)^{0.25}$	$8.0\,(f_{ck}/20)^{0.25}$	5.0	$5.5\,(f_{ck}/20)^{0.25}$
s_1	1.0 mm	1.8 mm	$s(\tau_{max})$[1]	$s(\tau_{max})$[1]	$s(\tau_{max})$[1]	$s(\tau_{max})$[1]
s_2	2.0 mm	3.6 mm	s_1	s_1	s_1	s_1
s_3	c_{clear}	c_{clear}	$1.2s_1$	c_{clear}	$1.2s_1$	c_{clear}
α	0.4	0.4	0.4	0.4	0.4	0.4
τ_f	$0.4\,\tau_{max}$	$0.4\,\tau_{max}$	0	$0.4\,\tau_{max}$	0	$0.4\,\tau_{max}$

1.) s_1 for splitting failure is calculated from the pull out failure bond curve for corresponding bond conditions.

According to the classification, the specimens should be subjected to splitting failure on both main bars and the strengthening bars. Bottom reinforcement and the mid reinforcement fall under the category of good bond conditions, see FIB (2010). In reality, corrosion affects the bond. First an analysis was run with a bond slip curve assuming uncorroded reinforcement; that curve was calculated from the fourth column in Table 4.1. Later on, the bond slip curves were altered to get the failure of beam with worse bond conditions, this curve was calculated from Table 4.2, based on the measured surface cracks. Clear rib spacing of the bars was considered to be 5.8 mm. Yielding of the reinforcement influences the bond as it leads to bond loss; therefore it is important taking the state of yielding into account, see Engström (1992). In these analyses, yielding was never reached and this assumption became unnecessary.

Table 4.2 The magnitude of the reduction in the residual bond strength for corroded reinforcement, from FIB (2010).

Corrosion penetration [mm]	Equivalent surface crack [mm]	Confinement	Residual capacity [%] Bar type	
			Ribbed	Plain
0.05	0.2-0.4	No links	50-70	70-90
0.10	0.4-0.8		40-50	50-60
0.25	1.0-2.0		25-40	30-40
0.05	0.2-0.4	Links	95-100	95-100
0.10	0.4-0.8		70-80	95-100
0.25	1.0-2.0		60-75	90-100
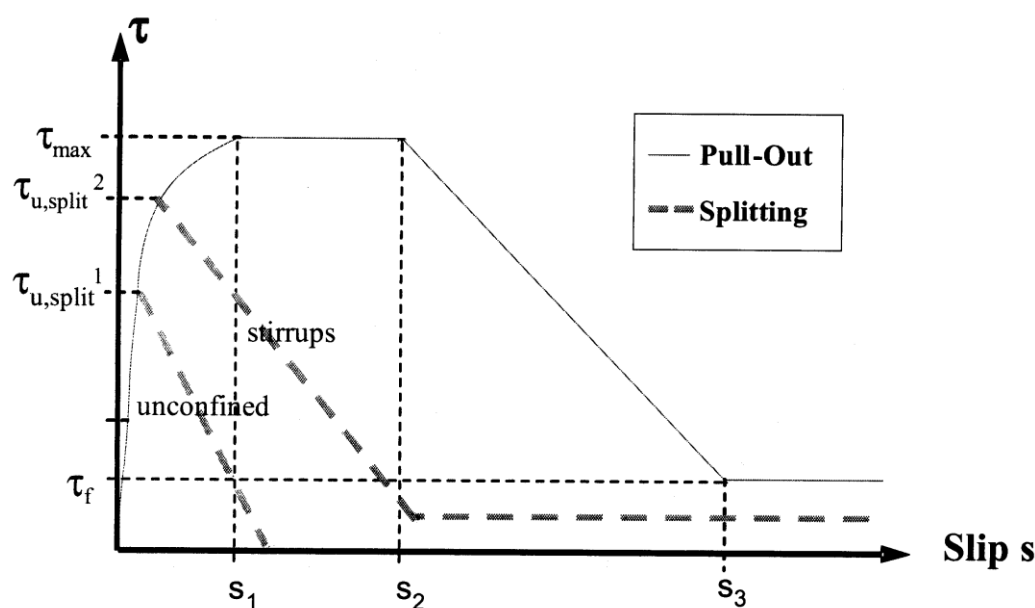
Figure 4.4 Bond slip curve, from FIB (2010).

4.3 Input data

Many analyses were performed just in order to get a closer response to reality. Two analyses were run with different compressive strength values for the concrete, one from the hammer test and the other from the cylindrical test, see chapter 3.3.1. The test with compressive strength from the hammer test showed lower ultimate capacity than the one from the cylindrical test. Therefore, it was decided to run further analysis with a value of 48 MPa for the compressive strength. This value is somewhere between the hammer test and cylindrical test values, but closer to the cylindrical test.

From that different analyses were run, changing other parameters, one at a time. The parameters that were changed were the bond curve, the tensile strength and the fracture energy. When estimating the fracture energy and tensile strength there were uncertainties that were needed to be taken into account, see chapter 3.3. Material parameters for the reinforcement were kept constant in all the analysis. Parameters used in the different analysis can be seen in Table 4.3.

Table 4.3   Input data for analysis.

Analysis number:	Concrete				Bond curve[1]
	f_{cm} [MPa]	f_{ctm} [MPa]	E_{cm} [GPa]	G_f [N/mm]	
I	49	3.6	35.2	0.147	A
II	44	3.27	34	0.144	A
III	48	3.5	35	0.147	A
IV[2]	48	3.5	35	0.147	A
V	48	2.7	35	0.147	A
VI	48	3.5	35	0.100	A
VII	48	2.7	35	0.100	A
VIII	48	3.5	35	0.147	B
IX	48	2.7	35	0.100	B
X[2]	48	2.7	35	0.100	A
XI[2]	48	2.7	35	0.100	B
XII[2]	48	2.7	35	0.100	C
XIII[2]	48	2.7	35	0.100	D

1.) Bond curve A corresponds to: splitting failure, good bond conditions and stirrups. Bond curve B is a modified version of bond curve A. Bond curves C and D correspond to bond curves A and B respectively, with reduced values to correspond to deterioration due to corrosion
2.) Unloading after the first bending cracks then loading until failure.

Both bond curves A and B were reduced for worst corrosion conditions according to Table 4.2. The bond curve used for the analysis can be seen in the Figure 4.5.
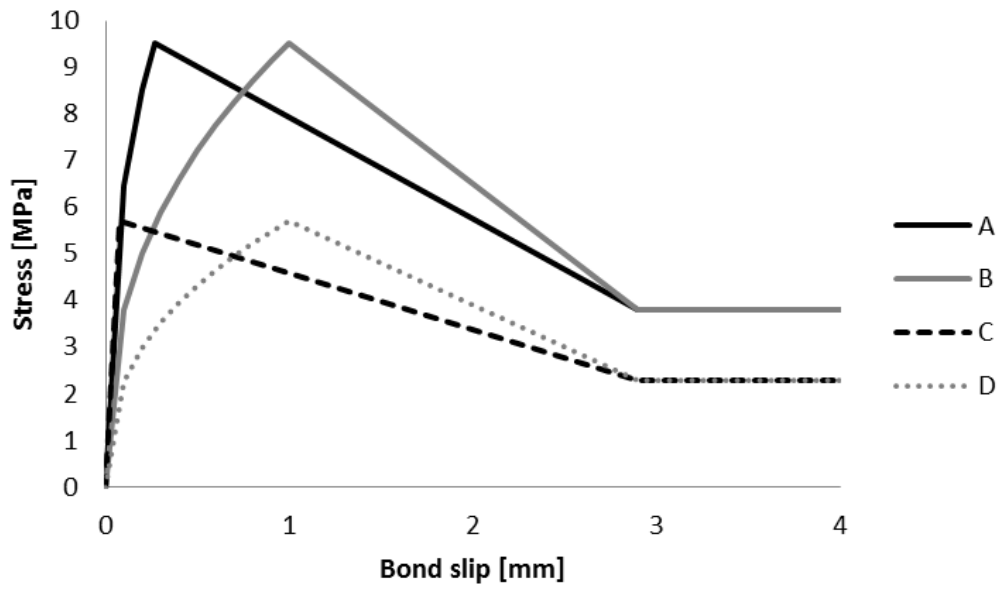
Figure 4.5 Bond curves used for the bottom strengthening in FE analysis.

4.4 Results

In Figure 4.6 and Figure 4.7, the behaviour of analysis I, II and III can be seen. The load deflection for the analyses follows the same behaviour but they have different ultimate load. As described in chapter 3.3.1, there are uncertainties in the material parameters. After consideration, it was decided to have analysis III as a reference analysis.

Figure 4.6 Load versus mid span deflection for analyses I, II and III.
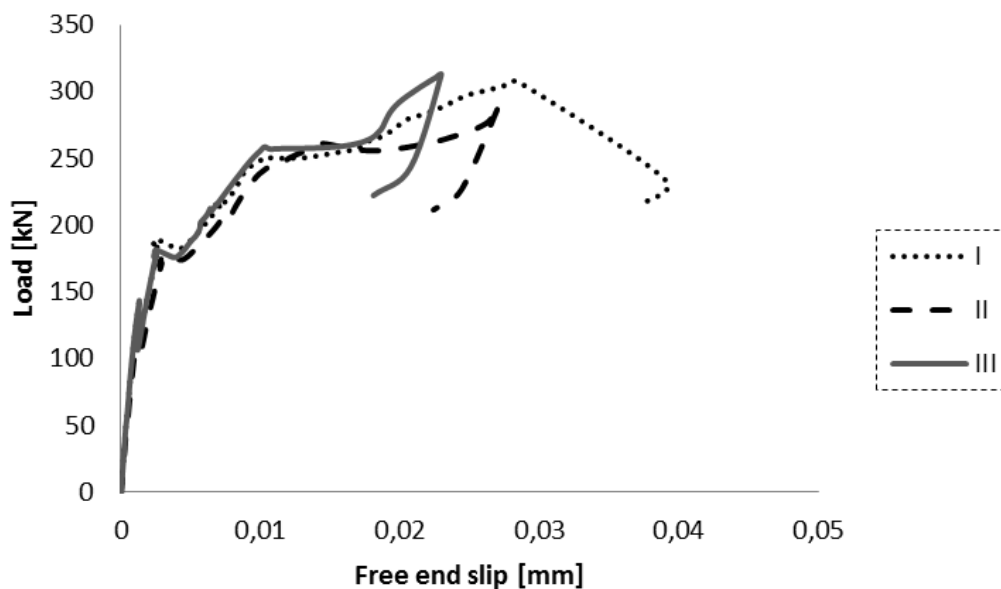
Figure 4.7 Load versus free end slip for analyses I, II and III.

The crack pattern for the reference analysis can be seen in Figure 4.3 which shows the equivalent total strain in the concrete at maximum load. The crack positions and cracking loads are related to Figure 4.8, Figure 4.9 and Figure 4.10 with numbers.
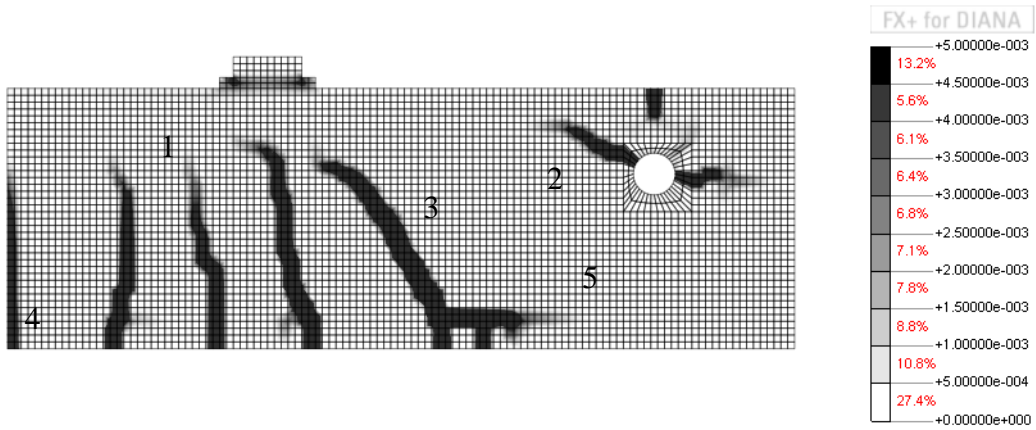
Figure 4.8 Crack pattern in terms of maximum principal tensile strains for maximum load in analysis III.
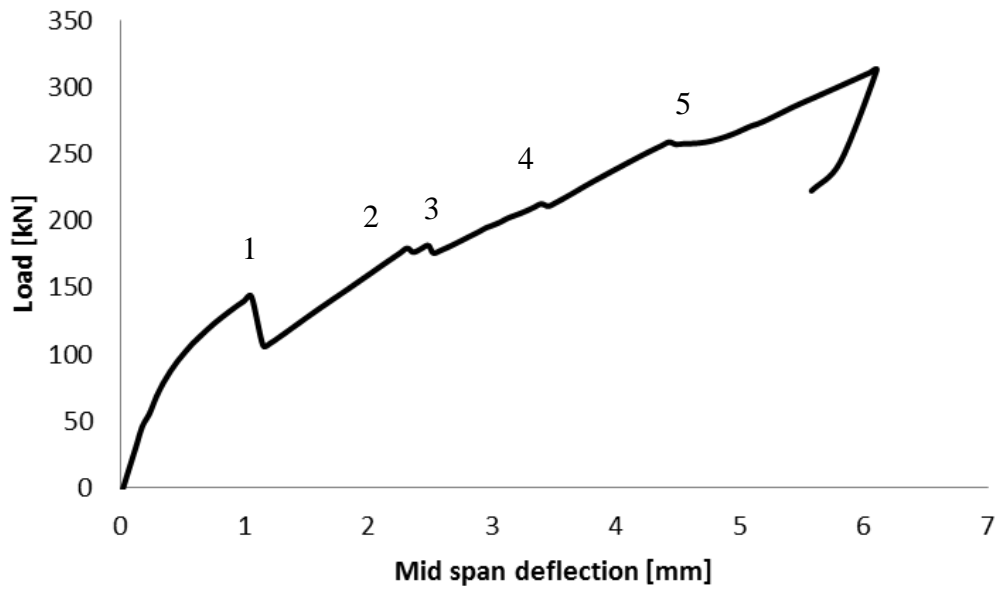
Figure 4.9 Load versus mid span deflection for the reference analysis III.
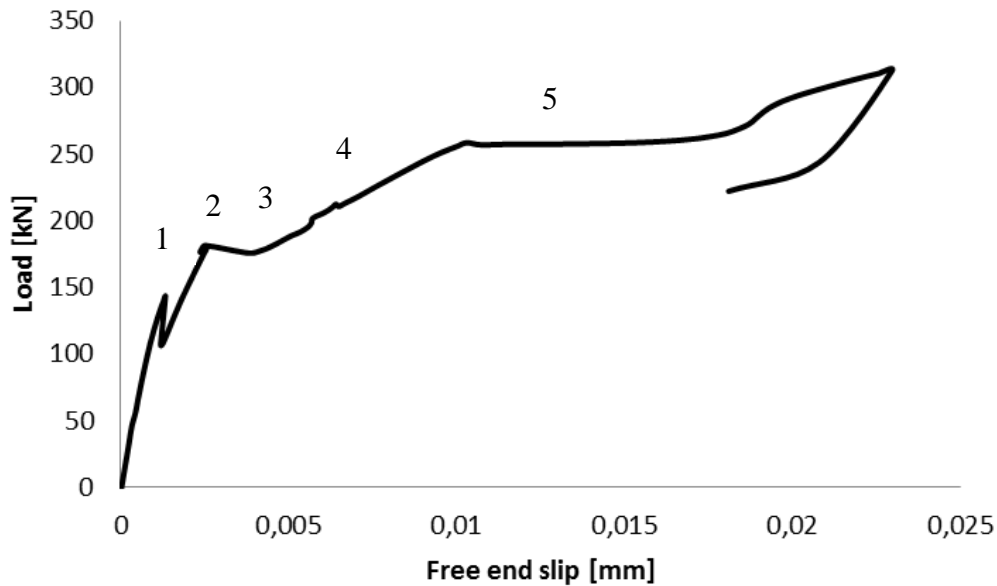
Figure 4.10 Load versus the free end slip for the reference analysis.

The first two cracks that opened were bending cracks, at a load of 143.1 kN (1). One of them was positioned in the midspan and the other crack was located under the load. Shear cracks around the support started to develop at a load of 179.2 kN (2). Shear crack developed in the shear span at a load of 181.4 kN (3). A bending crack in the middle of the beam opened at a load level of 212.3 kN (4). After the shear crack was formed, a crack along the bottom reinforcements opened, starting from the shear crack. The crack propagated to the end of the beam until failure. After reaching the load of approximately 255 kN, the stiffness of the beam decreased (5). That was when the crack opened along the bottom bar.

When the first two bending cracks opened, the load dropped. At that point the free end slip increased 0.0025 mm and when the final load was reached the free end slip was 0.023 mm.

After the first two bending cracks appeared, the stiffness of the beam was reduced to a great extent. Possibly, some of the test specimens from Stallbackabron already had some bending cracks, and would therefore, show lower initial stiffness. Therefore, analysis IV was run with an unloading phase so it would represent a cracked specimen. When the first two bending cracks had opened, the model was unloaded and then loaded to failure. The result from analysis IV can be seen in Figure 4.11 and Figure 4.12. By analyzing the force deflection graph, it can be seen that analysis IV lost stiffness in the beginning and then followed the same behaviour as the analysis III.
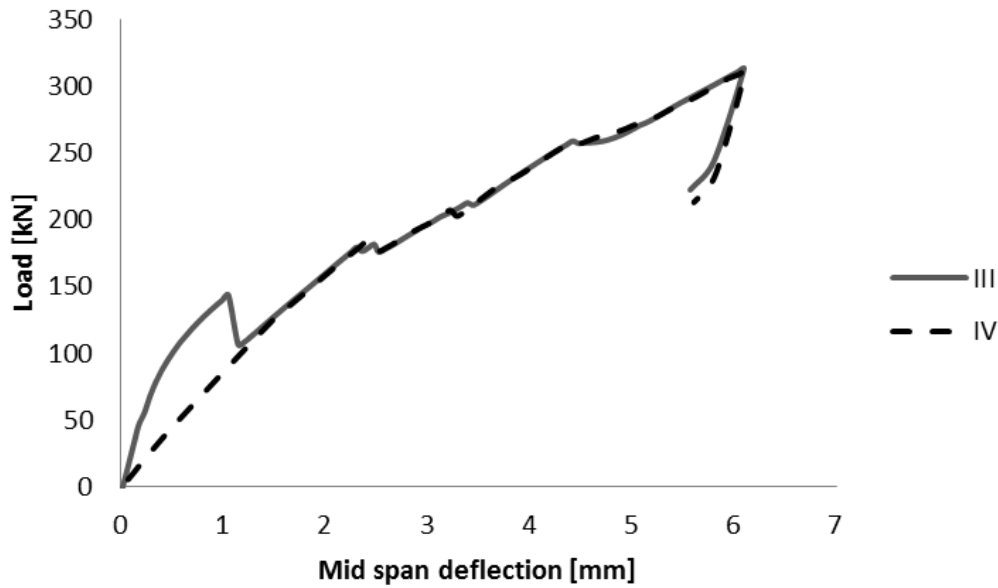
Figure 4.11 Load versus mid span deflection for analyses III and IV.
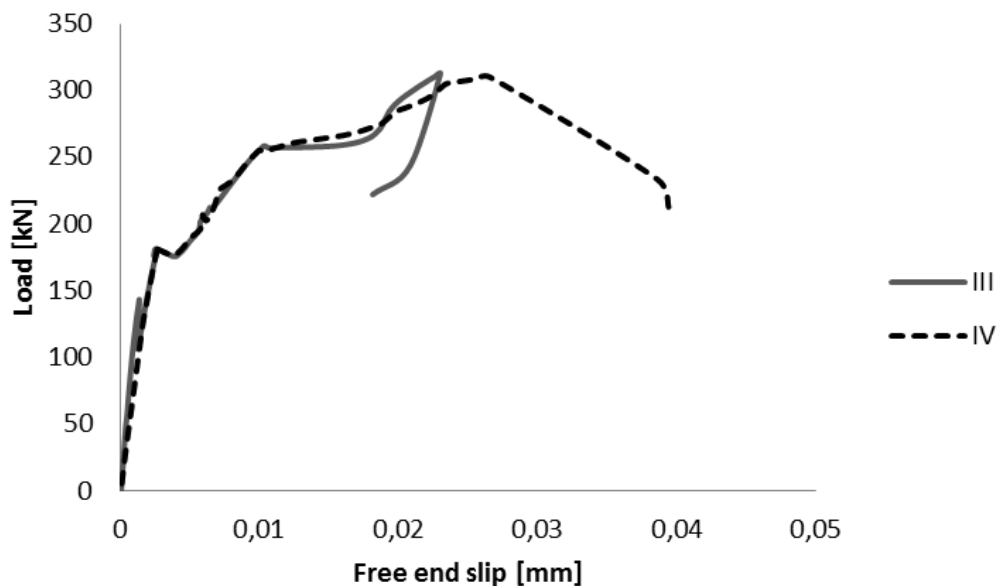
Figure 4.12 Load versus free end slip for analyses III and IV.

In analysis V, when the tensile strength of the concrete was decreased from 3.5 MPa to 2.7 MPa, a fourth bending crack developed between the first two around a load of 251 kN. The first bending crack developed for a slightly lower load; at 141.6 kN instead of 143.1 kN. The crack around the bottom reinforcement does not propagate as much as in the previous analysis. Besides that, the crack pattern was very similar. The V analysis reached slightly higher maximum load, 316.3 kN, resulting in a larger free end slip, 0.027 mm compared to 0.022 mm in analysis III.

In analysis VI, the fracture energy was lowered from 0.147 N/mm to 0.100 N/mm. The results were almost identical to analysis V, see Figure 4.13 and Figure 4.14.

In analysis VII, a combination of analysis V and VI showed interesting results. The first bending crack developed earlier and the beam showed a lower stiffness in general

compared to the other analysis. The main difference is that when maximum load was reached, a cracking around the bottom reinforcement started from the shear crack and propagated to the end of the beam. That resulted in a larger free end slip of the reinforcement, 0.13 mm. The ultimate load was also lower in analysis VII than the others, 266 kN compared to around 315 kN for the others. Comparison between analysis III, V, VI and VII can be seen in Figure 4.13 and Figure 4.14.
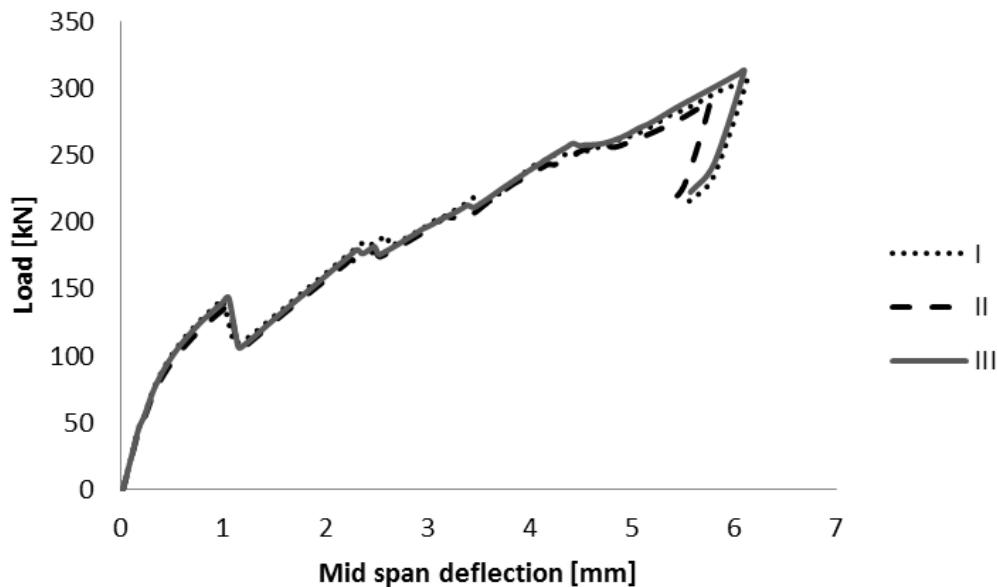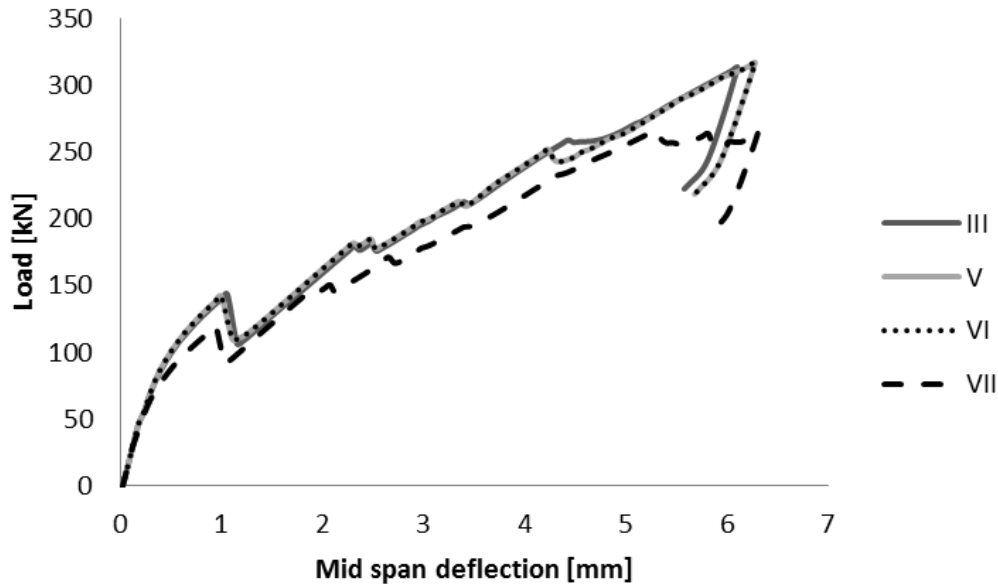

Figure 4.13 Load versus mid span deflection for analyses III and V-VII.
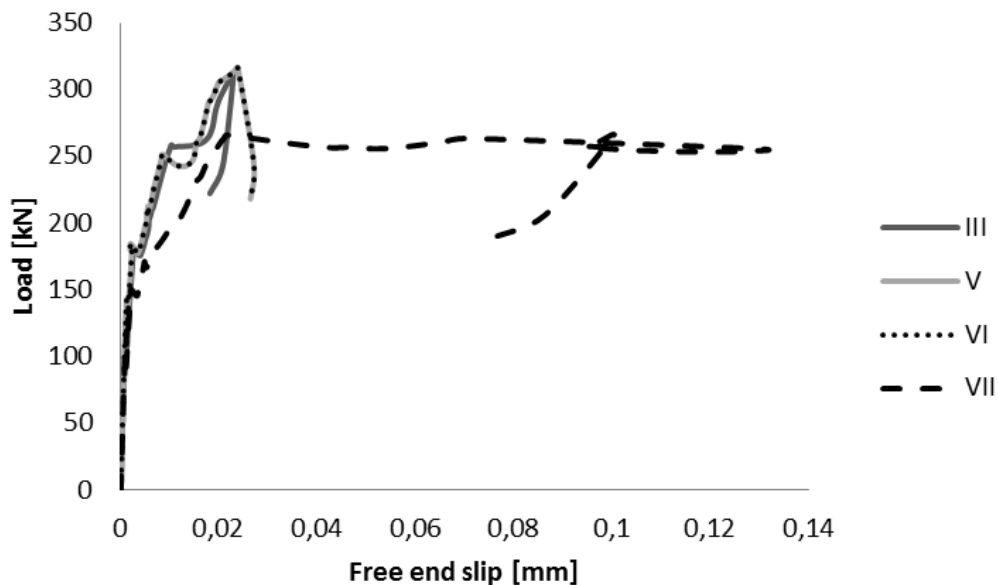
Figure 4.14 Load versus free end slip for analyses III and V-VII.

Even though we have FIB (2010) to develop the bond curves, it is quite uncertain that the curves fit the reality therefore, analysis VIII was performed with another bond curve. The new bond curve B was developed, similar to bond curve A but with less stiffness see Figure 4.5. The results were the same as the analysis III up to 180 kN but after that the beam showed lower stiffness. Analysis IX was a combination of the

analysis VII and VIII, see comparison of analysis III, VIII and IX in Figure 4.15 and Figure 4.16.
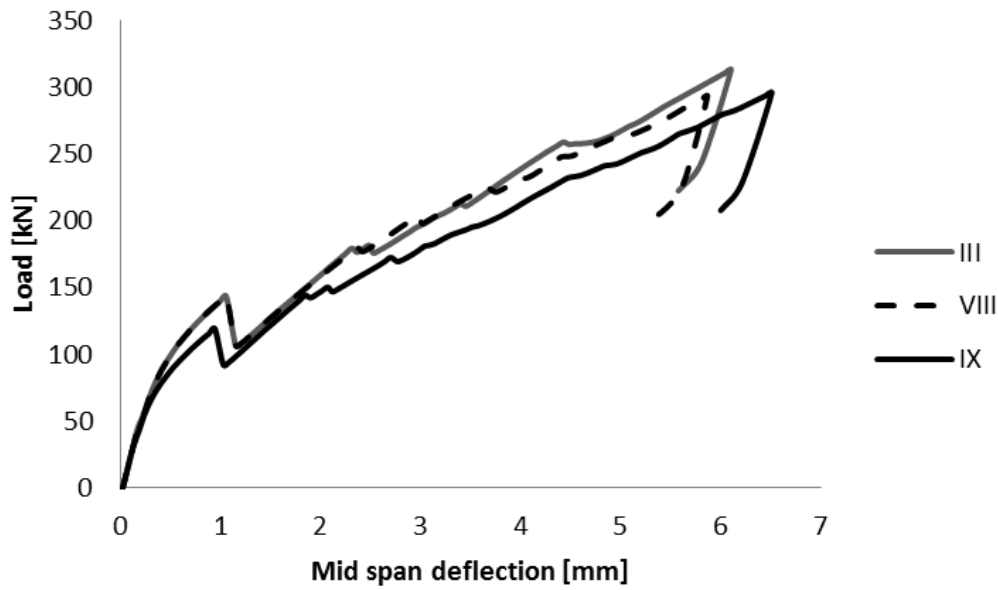
Figure 4.15 Load versus mid span deflection for analyses III, VIII and IX.
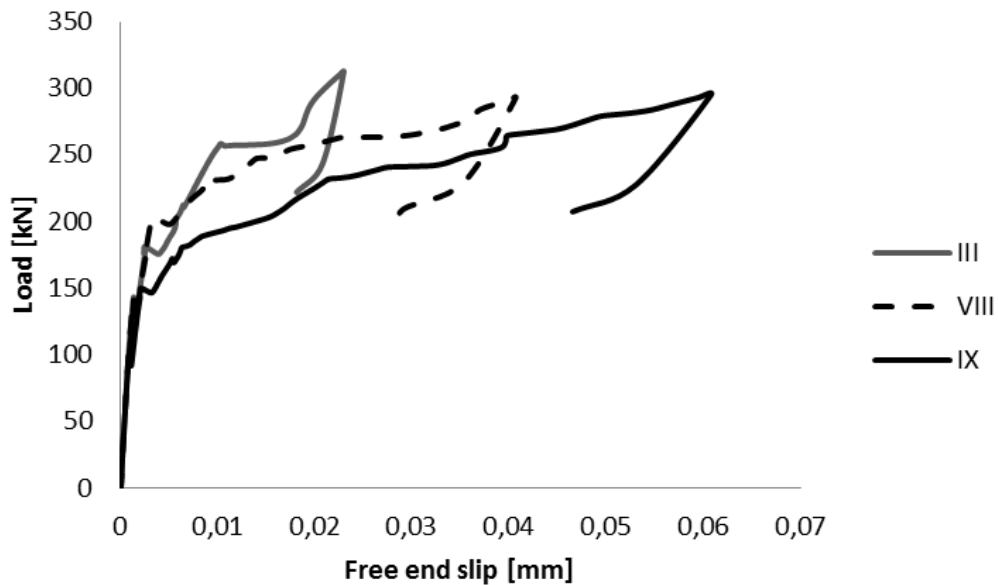
Figure 4.16 Load versus free and slip for analyses III, VIII and IX.

Analysis X and XIII were run in order to adjust the bond slip curve in an attempt to get the appropriate behaviour of the bond slip. Comparison can be seen in Figure 4.17 and Figure 4.18.
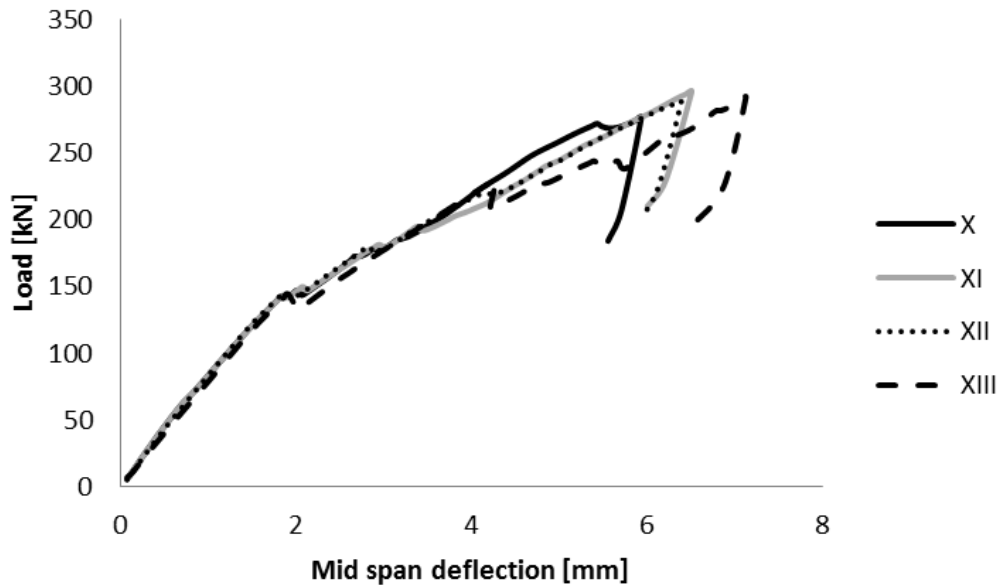
Figure 4.17 Load versus mid span deflection for analyses X-XIII.
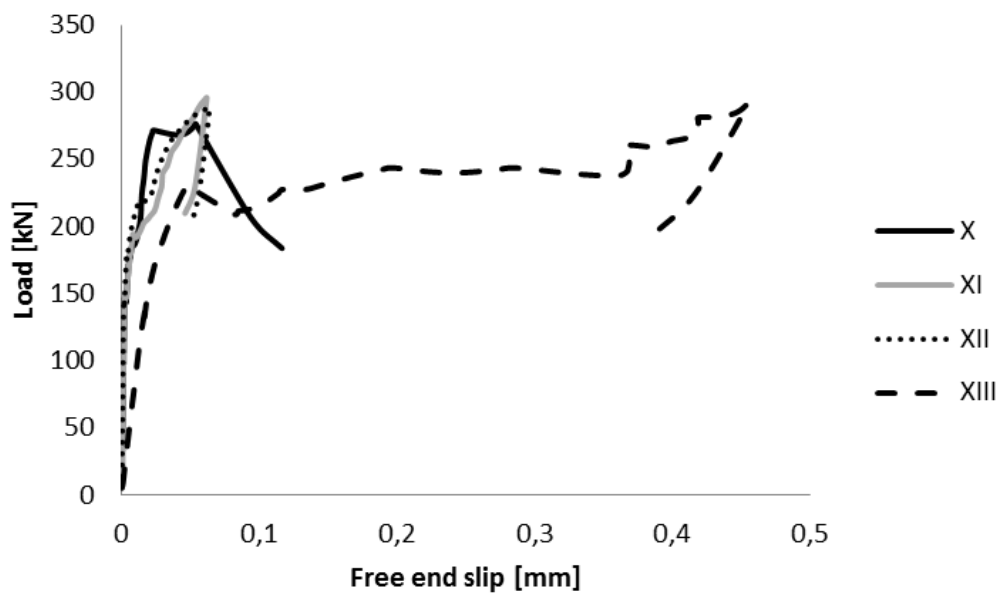
Figure 4.18 Load versus free end slip for analyses X-XIII.

Results from all the analyses were put together in Table 4.4. Analyses XII and XIII correspond to a medium damaged specimen with a crack width of at least 1.0 to 2.0 mm or highly damaged specimen.

Table 4.4 Results for FE analysis.

Analysis	Max. load [kN]	Max. deflection [mm]	Max. free end slip [mm]
I	307.3	6.1	0.039
II	290.4	5.9	0.027
III	312.6	6.1	0.023
IV	310.2	6.1	0.039
V	316.3	6.3	0.027
VI	316.3	6.3	0.027
VII	265.9	6.3	0.131
VIII	292.9	5.9	0.041
IX	293.5	6.5	0.061
X	276.3	5.9	0.116
XI	295.8	6.5	0.062
XII	288.3	6.4	0.064
XIII	291.4	7.1	0.456

5 Comparison of experimental and FE analysis results

The comparision between the 2D non-linear FE analyses and experimental results comes in two parts; firstly, the behaviour of the reference specimen is compared to the FE analysis and secondly the medium specimens are compared.

5.1 Comparision for the reference specimen

By looking at Figure 5.1, it can be seen that there is a very good correlation between analysis VII and specimen R6. In the beginning, analyses VII shows a bit stiffer behaviour, that can be explained by the fact that the specimens are already cracked. After the first crack develops in analyses VII, the curve follows a same trend as specimen R6, the ultimate load is however much lower in analysis VII than in specimen R6. Analyses III and IV have similar ultimate load as specimen R6 but with higher stiffness.
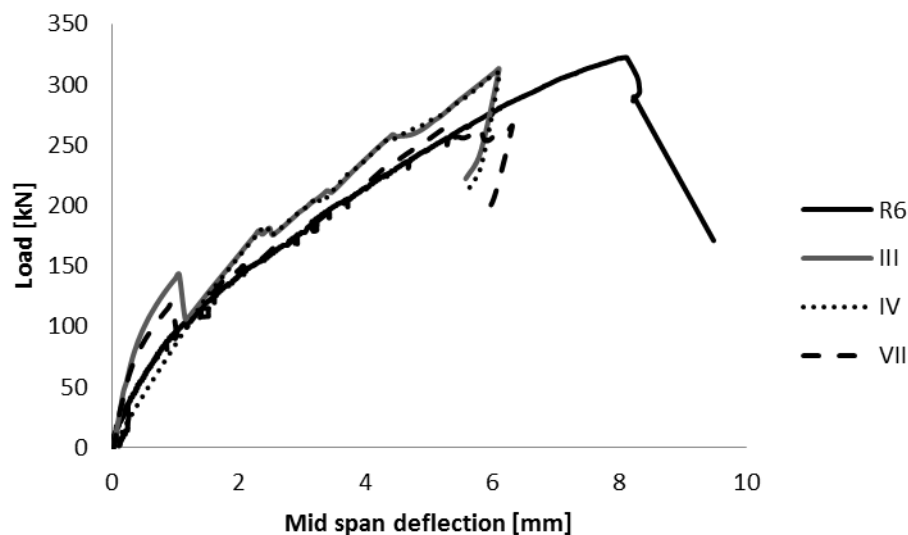
Figure 5.1 Load versus mid span deflection.

First bending crack was observed in specimen R6 for a load level of 85 kN; however in the analyses, it was for slightly larger loads: 118 kN in analyses VII and 143 kN for analyses III and IV. Shear cracks started developing in specimen R6 for a load level of 160 kN; in analysis VII, it was 145,5 kN and in analyses III and IV 181 kN. Thus, the load level causing the shear cracks agreed rather well on an average.
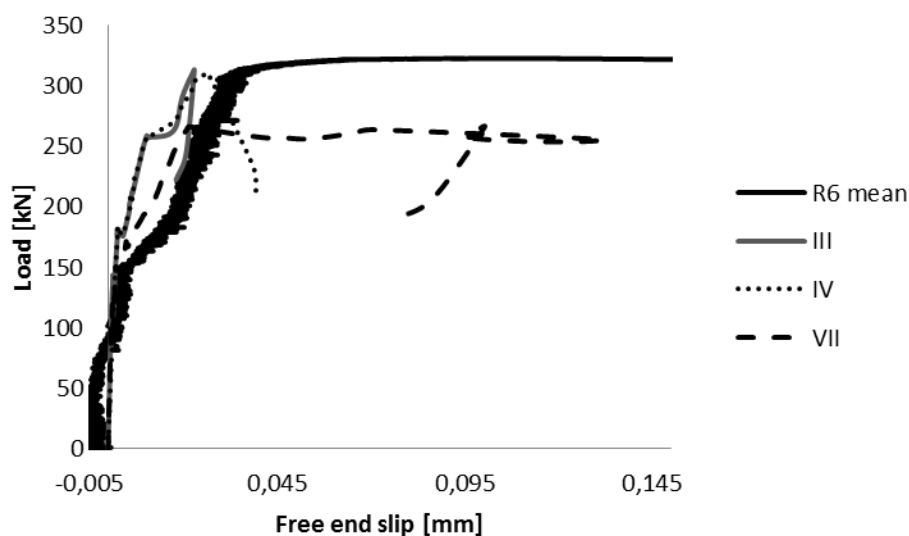
Figure 5.2 Load versus free end slip.

The free end slip from analysis VII follows specimen R6 better than the free end slip in analyses III and IV. In fact, it gives quite accurate results, see Figure 5.2. The maximum slip was much smaller in all analyses than the slips observed in the tests. This can possibly be explained by the fact that the available anchorage length was 530 mm in all the analyses but for specimen R6 it was 435 mm. If a second shear crack would have formed in the FE analyses as it did in the experiments it probably might have resulted in a better correspondence between the free end slip values in analyses and the experiments. Another reason might be that the analyses become unstable and therefore, higher values of end slip never reached.

5.2 Comparision for the medium specimens

By looking at Figure 5.3, it can be seen that there is also a very good correlation between the medium damaged specimens and analyses XII and XIII. For low load levels, the medium specimens are slightly stiffer, that can be explained by the fact that the analyses were unloaded after first bending cracks occurred and then loaded again to represent cracked specimen. The ultimate load was slightly higher in the analyses but the behaviour is almost the same up to the failure load.
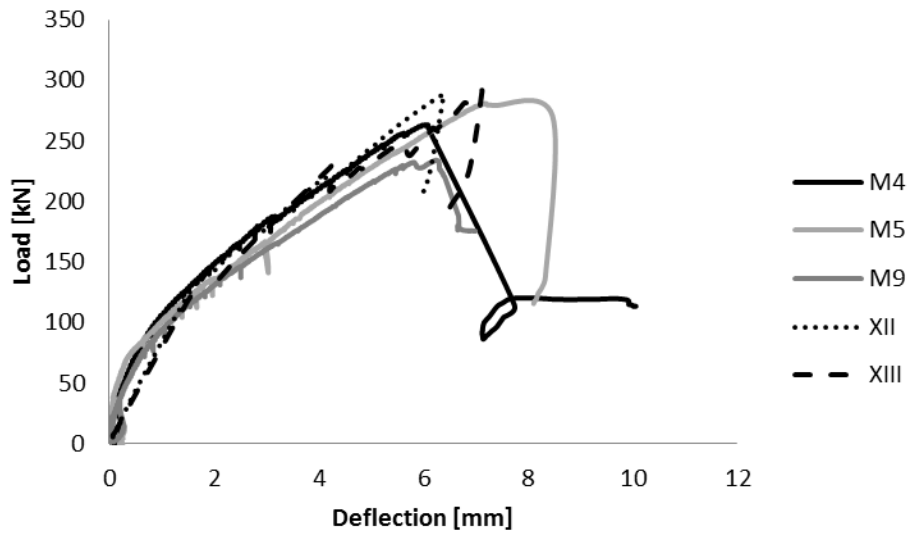
Figure 5.3 Load versus mid span deflection.

The first bending cracks in the experiments were observed at a load level of 92, 105 and 115 kN. In the analyses, it was for load 122 kN in XII and 115 kN in XIII; thus, they were rather close to the test measurements. The shear cracks were observed in the experiments at load levels of 120, 155 kN, and 175 kN. In the analyses they appeared at loads of 144 kN in XII and 230 kN in XIII. The bending cracks appeared at similar load levels in the two discussed analyses, while the load needed to propagate the shear crack was much greater in analysis XIII than in XII. With regard to cracking load, analysis XII described the tests results in a better way.
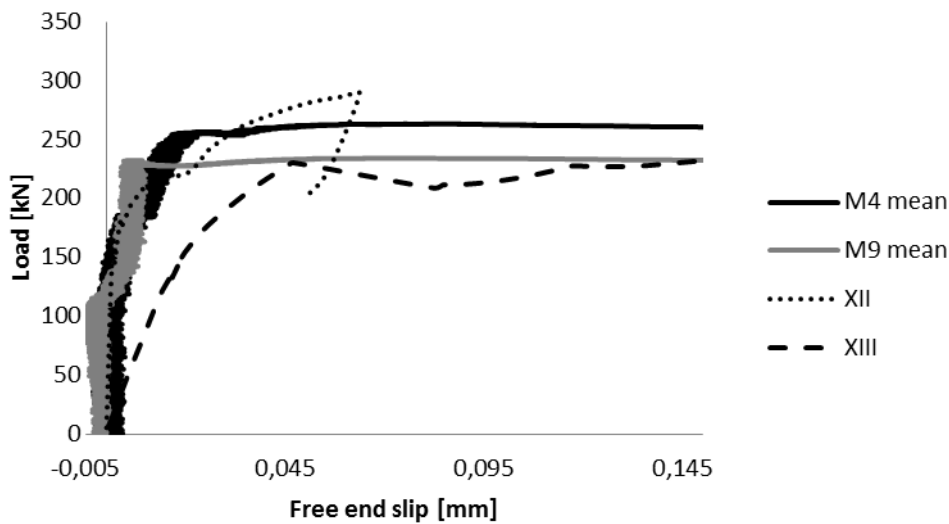
Figure 5.4 Load versus free end slip, enlarged.
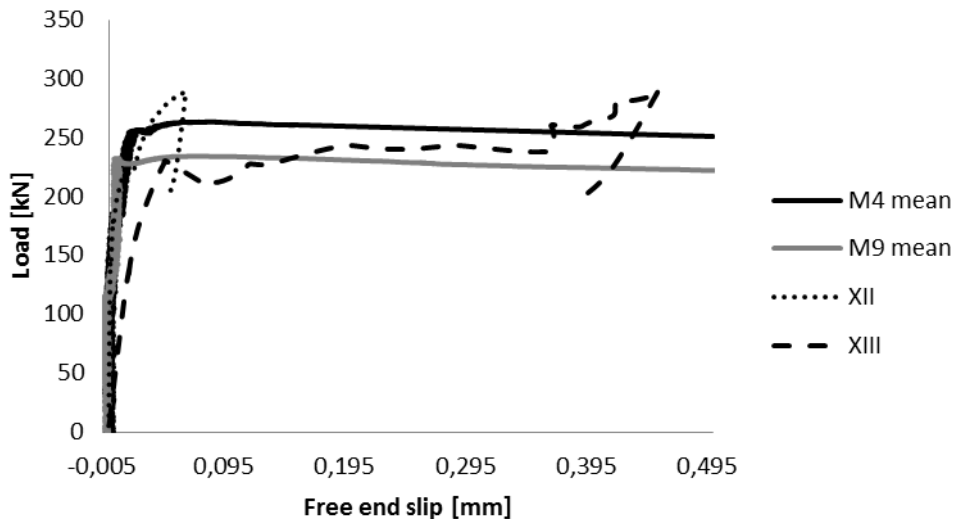
Figure 5.5 Load versus free end slip.

The free end slip for analysis XII follows the measured ones better in the beginning than the free end slip for analysis XIII, *Figure 5.4*. However for higher slip values, analysis XIII captures better the actual behaviour of the beams, see Figure 5.5. As for the reference specimen the maximum slip values are much smaller for all the analyses than what was observed in the test. That can possibly be explained by the fact that the available anchorage length was 530 mm in all the analyses but for the medium damaged specimens it was from335 mm to 435 mm. If a second shear crack would have formed in the FE analyses as it did in the experiments. It might have resulted in a better correspondence in the free end slip, between the analyses and the experiments for high values of slip after failure. Another reason is that the analyses become unstable and a high value of free end slips are never reached because of that.

5.3 Discussion of comparisions

When analyses and the tests were compared, there was a good correlation between:

- Force versus mid span displacement
  - Maximum load
  - Stiffness
- Load at first cracking
- Behaviour for free end slip at failure

However there was not a good correlation between:

- Behaviour for free end slip after failure
- The final crack pattern
- Available anchorage length

When comparing reference specimen analyses, VII fitted the test results best. Analysis VII had reduced tensile strength and the fracture energy in order to take the ageing and deterioration of the concrete into account. If an unloading phase would have been added, it would show the same behaviour in the beginning as the test did. When comparing medium damaged specimen analyses, XII fitted the test results best. Analysis XII also had reduced tensile strength and fracture energy to take into account

ageing and deterioration of the concrete; furthermore it had reduced maximum bond strength to take into account the effect of corrosion on the bond. Thus, the only difference between the analysis that fitted reference specimen and medium specimens best was the bond curve. It is interesting to note that between a reference specimen and medium damaged specimen in the analyses, it was only the maximum bond stress that changed. The same material parameters were used for the concrete independent of the level of corrosion.

Maximum load, stiffness, load level for cracking and behaviour of free end slip at failure showed good correlation. However, the free end slip at a given load level was smaller in the analyses than in the tests. That is probably related to the crack pattern; in the analyses, only one shear crack was observed, while in the tests, there were usually two shear cracks. Subsequently, the available anchorage length was longer in the analyses, which is a probable explanation for the stiffer load versus free end slip behaviour in the analyses.

Many different analyses were carried out, trying to obtain a second shear crack also in the analyses. Several parameters were varied; it was not considered necessary to include all details in the report. Some examples of what was tried are as the following:

- To reduce the area of stirrups and/or to skip the stirrups totally, in order to see if the stirrups had any effects on the shear strength of the specimens.
- To use a linear softening curve for the concrete in tension, instead of the curve described by the expression of Hordijk.
- To include the effect of lateral confinement with the model proposed by Selby and Vecchio.
- To decrease the capacity in tension if the concrete is simultaneously loaded in tension in perpendicular direction according to the model by Vecchio and Collins.

None of the different analyses resulted in more promising crack pattern. Chen and Du (2012) had similar problems in non-linear 3D FE analysis of reinforced concrete beams loaded in four point bending. By including the effect of lateral confinement they succeeded to get a second shear crack in their analyses. However, as stated earlier, that did not have the same effect in the analyses carried out in this study; the main explanation is likely that the effect of lateral confinement was more important in 3D models than in 2D models.

It would have been interesting, in order to verify that a shear crack closer to the end would result in higher values of the free end slip, to locally weaken elements at a position where a shear crack is wanted.

6 Conclusions

The aim of this thesis was to gain better understanding of the structural effects of naturally corroded reinforcement, and especially to investigate bond in naturally corroded concrete structures. This was done with experimental work on 5 specimens from Stallbackabron in Trollhättan with regard to anchorage capacity, development of a 2D non-linear finite element model of a specimen and comparison of the two. The specimens were prepared both at site and in the laboratory. On site they were chosen from a large sample of specimens that had earlier been documented with regard to crack width. 5 specimens were tested.

The five specimens were one reference specimens and four specimens with medium damage. The specimens were tested in a four point bending test which was designed to capture anchorage failure. The displacements of the specimens and the main reinforcement were measured with several LVTD:s. Four of the specimens failed by anchorage failure of the main bars, while the last one, which was severely cracked along the main reinforcement before testing, failed by lack of anchorage of the strengthening bars.

In the analyses, both the bond and the material parameters were adjusted to capture the behaviour of the test specimens in the tests. The results from the non-linear 2D finite element analysis showed good correlation to the results from the experiments regarding the maximum load and deflection. When describing the level of corrosion with the FE analyses, a change of the maximum bond stress was sufficient.

The non-linear 2D finite element analysis did not show sufficient results with regard to free end slip of the main reinforcement of the test specimens. In all the tests, a large value of free end slip was reached after failure but in the analyses the values of free end slip always decreased after failure.

Furthermore there were differences in the obtained crack patterns in the tests and the analyses; although there were some major similarities. In both cases, the first crackings were bending cracks followed by shear cracks around the supports. The position of the main shear crack was similar in both cases but in the tests we got a second shear crack which led to a shorter anchorage length in the tests than in the analyses. If the formation of the second shear crack would have been reached in the analyses, a larger value of free end slip might have been reached after the failure.

It should be noted that the crack pattern observed in the experiments cannot be completely described by a 2D model. For instance, we have splitting cracks in all of the tests and in some cases the splitting cracks on the sides and the bottom were connected and led to spalling of the concrete around the corners.

The following conclusions can be drawn:

- 2D analysis shows sufficient results regarding maximum load and deflection.
- 2D analysis does not show sufficient results regarding free end slip and crack pattern.
- Lowering the fracture energy and the tensile stiffness of the concrete in the analyses resulted in better agreement.
- Adjusting the bond curve to be weaker than given in FIB (2010) and with lower bond stress for corroded reinforcement, see FIB (2010), resulted in better agreement.
- Higher degree of corrosion resulted in lower ultimate load.

- Longer available anchorage length resulted in higher ultimate load.
- The ultimate load was not connected to at which load the first flexural or shear crack appears.
- The free end slip of the main bars starts at a load of 90 - 97% of the maximum load

7   References

Berg F. and Johansson D. (2011): *Design of Test Set-up using FEM*. Master Thesis, Department of Civil and Enviromental Engineering, Chalmers, Göteborg, 2011, pp. 43.

Broomfield J. P. (1997): *Corrosion of Steel in Concrete - Understanding, investigation and repair*, E & FN Spon, London, Great Britain, 1997, pp.

Browne R. D. (1985): Practical considerations in placing durable concrete. *Proceedings of Seminar on Iprovements in Concrete Durability*, pp. 97-130.

Chen N. and Du H. (2012): *Detailed Study of Cracking Process at Shear Failure through FE Analysis of Beam Experiments*. Msc, Department of Civil and Enviromental Engineering, Chalmers, Göteborg, 2012, pp. 95.

Domone P. and Illston J. (2010): *Construction Materials - Their Nature and Behaviour*, Spoon Press, Abington, 2010, pp.

Engström B. (1992): *Ductility of Tie Connections in Precast Structures*. Division of Concrete Structures Chalmers University of Technology, Göteborg, 1992, pp. 452.

FIB (1993): *Model Code 1990*. International Federation for Structural Concrete, Lausanne, Switzerland, pp. 437.

FIB (2000): *Bond of reinforcement in concrete, State of the are report*. International Federation for Structural Concrete, Lausanne, Switzerland, pp. 427.

FIB (2010): *Model Code 2010*. International Federation for Structural Concrete, Lausanne, Switzerland, pp. 292.

Hanjari K. Z. (2010): *Structural Behaviour of Deteriorated Concrete Structures*. Department of Civil and Enviromental Engineering, Divison of Structural Engineering, Concrete Structures, Chalmers University of Technology, Gothenburg, 2010, pp. 64.

Jirsa J. O., Chen W., Grant D. B. and Elizondo R. (1995): *Development of bundled reinforcing steel*. Center for transportation research Univeristy of Texas at Austin, Texas USA.

Lundgren K. (2007): Effect of corrosion on the bond between steel and concrete: an overview. *Magazine of Concrete and Research*, Vol. 59, No. 6, pp. 447-461.

M. Tahershamsi K. Z. H., K. Lundgren, M. Plos (2012): Anchorage in naturally corroded specimens taken from existing structures.

Magnusson J. (2000): *Bond and Anchorage of Ribbed Bars in High-Strength Concrete*. Division of Concrete Structures, Chalmers University of Technology, Göteborg, Sweden, 2000, pp. 300.

Müller H. S. (2009). "Constitutive modelling of high-strength/high-performance concrete." Israel bi-annual Conference for Structural Engineering, Universität Karlsruhe (TH) Institute of Concrete Structures and Building Materials, Tel Aviv.

Sæther I. (2011): Bond deterioration of corroded steel bars in concrete. *Structure and Infrastructure Enineering*, Vol. 7, No. 6, 29 July 2009, pp. 415-429.

Tepfers R. (1973): *A Theory of Bond Applied to Overlapped Tensile Reinforcement Splices for deformed Bars*. Division of Concrete Structures, Chalmers University of Technology, Göteborg, Sweden, 1973, pp. 328.

Val D. V., Stewart M. G. and Melchers R. E. (1998): Effect of reinforcement corrosion on reliability of highway bridges. *Engineering Structures*, Vol. 20, No. 11, pp. 1010-1019.

Appendix A. Stress strain relationship of steel rebars

Ks40

STÅLPROTOKOLL   löp.nr.................

LEVERANTÖR : ....

KVALITET : ⌀10 Ks40...............

KVANTITET : ....

INTERN BETECKNING-MÄRKE(=lev.datum):.....................

   —"—   —"—   -FÄRG : RÖD................................

ANTAL PROVSTÄNGER : 5 st. (medelvärden enl. nedan)

ARBETSDIAGRAM:

MATERIALDATA:				ANMÄRKNINGAR
DIAMETER	Φ	mm	10,02	
STRÄCKGRÄNS	σ_{su}	kp/cm²	467,93	
BROTTGRÄNS	σ_B	kp/cm²	638,47	
STRÄCKTÖJNING	ε_s	‰	2,27	
BROTTÖJNING	ε_q	‰	11,4	
FÖRLÄNGNING	δ	‰		
ELASTICITETSMODUL	E	kp/cm²	206	
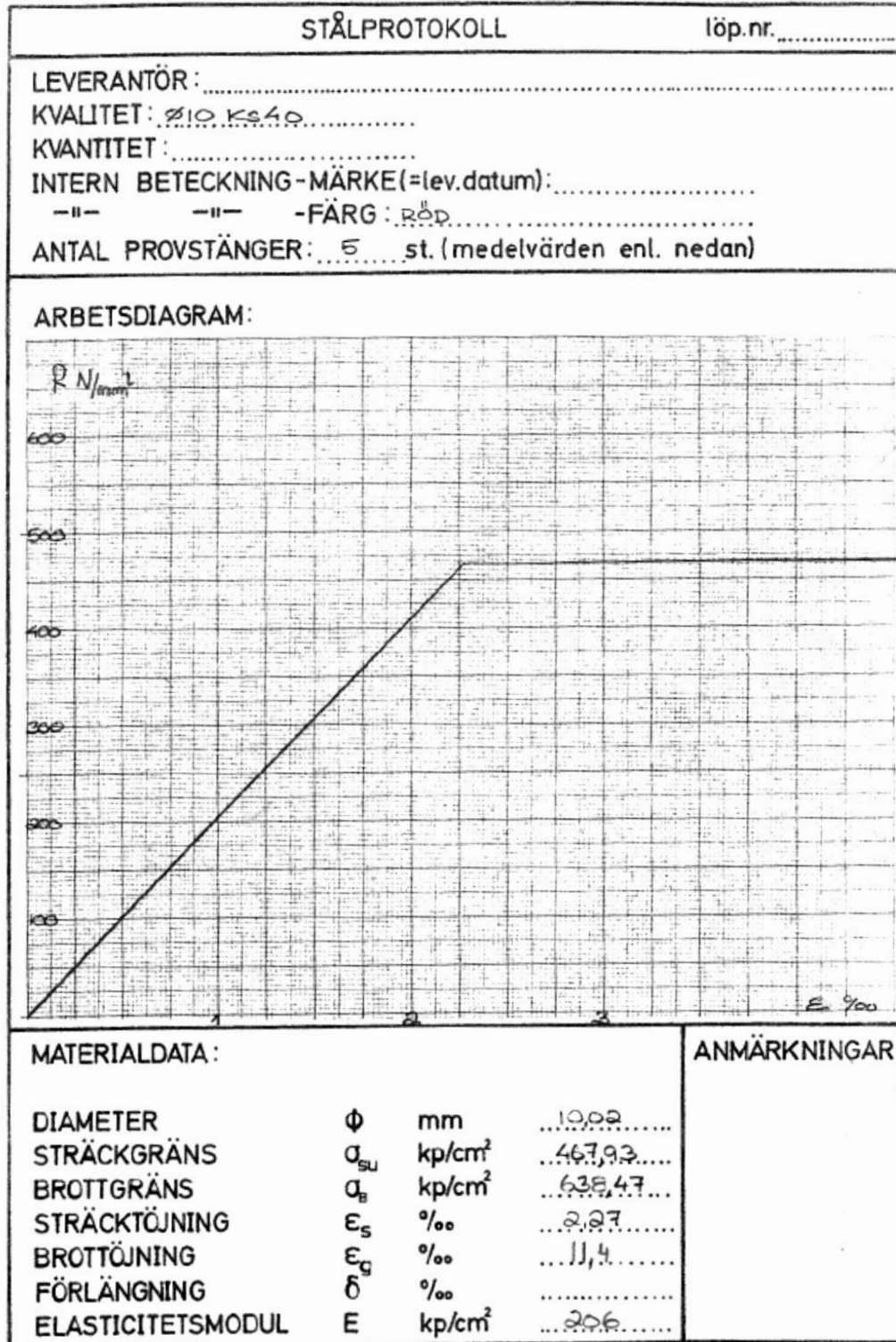
Ks60

STÅLPROTOKOLL   löp.nr. ....

LEVERANTÖR: .... Halmstad ....
KVALITET: .. Ø 16 Ks 60 ....
KVANTITET: ....
INTERN BETECKNING-MÄRKE(=lev.datum): ....
—"—   —"—   -FÄRG: ...... Blå ....
ANTAL PROVSTÄNGER: ... 5 ... st. (medelvärden enl. nedan)

ARBETSDIAGRAM:

MATERIALDATA:

DIAMETER	Φ	mm	15.8
STRÄCKGRÄNS	σ_{su}	kp/cm²	693.13
BROTTGRÄNS	σ_{B}	kp/cm²	906.63
STRÄCKTÖJNING	ε_{s}	⁰/₀₀	3.12
BROTTÖJNING	ε_{g}	⁰/₀₀	12.5
FÖRLÄNGNING	δ	⁰/₀₀	
ELASTICITETSMODUL	E	kp/cm²	222

ANMÄRKNINGAR

Appendix B.   Data file for FE analysis

```
Translated from FX+ for DIANA neutral file (version 1.2.0).
'DIRECTIONS'
   1  1.00000E+000   0.00000E+000   0.00000E+000
   2  0.00000E+000   1.00000E+000   0.00000E+000
   3  0.00000E+000   0.00000E+000   1.00000E+000
'COORDINATES'
   1  9.75600E+002   2.55000E+002   0.00000E+000
   2  9.87800E+002   2.52500E+002   0.00000E+000
   3  1.00000E+003   2.50000E+002   0.00000E+000
 .
 .
 .
4975  8.80000E+002   3.60000E+002   0.00000E+000
4976  8.80000E+002   3.70000E+002   0.00000E+000
4977  8.80000E+002   3.80000E+002   0.00000E+000
```

Definitions of directions (brace for directions block)

Coordinates for nodes (brace for coordinates block)

Material properties input

```
'MATERI'
   1 NAME    "Concrete"
     YOUNG   3.46000E+004                          Young modulus
     POISON  2.00000E-001                          Poisson ratio
     DENSIT  2.40000E-006                          Density
     TOTCRK ROTATE                                 Rotating cracks
     TENCRV HORDYK                                 Tension curve
     TENSTR  3.40000E+000                          Tensile strength
     GF1     1.45000E-001                          Fracture energy
     CRACKB  1.00000E+001                          Crack band width
     COMCRV THOREN                                 Compressive curve
     COMSTR  4.6000E+001                           Compressive strength
   2 NAME    "Interface"
     DSTIF   4.00000E+001  4.00000E+001            Dummy stiffness
     BONDSL 3                                      Multi linear bond-slip curve
     SLPVAL  0.00000E+000  0.00000E+000  4.81129E+000  4.25000E-002
             6.34853E+000  8.50000E-002  7.46638E+000  1.27500E-001
             8.37694E+000  1.70000E-001  9.15903E+000  2.12500E-001
             9.85194E+000  2.55000E-001  3.94078E+000  2.90000E+000
             3.94078E+000  1.00000E+001            Values for bond slip curve
   3 NAME    "Reinforcement"
     DENSIT  7.80000E-006                          Density
     YOUNG   2.22000E+005                          Young's modulus
     POISON  3.00000E-001                          Poisson ratio
     YIELD  VMISES                                 Yield criteria
     HARDEN STRAIN                                 Strain hardening
     HARDIA  6.93130E+002 0.00000E+000 9.06830E+002  1.25000E-001
```
        Yield stress   **Yield strain**   **Ultimate stress**   **Ultimate strain**

```
4 NAME    "Stirrup"
     DENSIT  7.80000E-006
     YOUNG   2.06000E+005
     POISON  3.00000E-001
     YIELD  VMISES
     HARDEN STRAIN
     HARDIA  4.68000E+002 0.00000E+000 6.38000E+002  1.40000E-001
   5 NAME    "Strengthening"
```

```
       YOUNG   2.06000E+005
       POISON  3.00000E-001
       DENSIT  7.80000E-006
       YIELD   VMISES
       HARDEN  STRAIN
       HARDIA  4.68000E+002 0.00000E+000  6.38000E+002 1.14000E-001
   6 NAME    "DummySuspension"
       DENSIT  0.00000E+000
       YOUNG   1.95600E+011
       POISON  3.00000E-001
   7 NAME    "WoodBoard"
       YOUNG   1.60000E+003
       POISON  3.50000E-001
       DENSIT  6.00000E-007
   8 NAME    "SteelPlate"
       YOUNG   2.10000E+005
       POISON  3.00000E-001
       DENSIT  7.80000E-006
       YIELD   VMISES
       HARDEN  STRAIN
       HARDIA  4.90000E+002 0.00000E+000  6.30000E+002 1.14000E-001
   9 NAME    "Strength"
       YOUNG   2.06000E+005
       POISON  3.00000E-001
       DENSIT  7.80000E-006
       YIELD   VMISES
       HARDEN  STRAIN
       HARDIA  4.68000E+002 0.00000E+000  6.38000E+002 1.14000E-002
  10 NAME    "Interface2"
       DSTIF   4.00000E+001  4.00000E+001
       BONDSL 3
      SLPVAL  0.00000E+000  0.00000E+000  4.97634E+000  1.00000E-001
              6.56632E+000  2.00000E-001  7.72251E+000  3.00000E-001
              8.66431E+000  4.00000E-001  9.47323E+000  5.00000E-001
              1.01900E+001  6.00000E-001  1.08380E+001  7.00000E-001
              1.14326E+001  8.00000E-001  1.19842E+001  9.00000E-001
              1.25000E+001  1.00000E+000  1.25000E+001  3.00000E+000
              5.00000E+000  5.80000E+000  5.00000E+000  1.00000E+001
```

Geometry and data properties input

```
'GEOMET'
   1 NAME   "Interface"                    Bottom bars
       THICK   1.80864E+002                Circumference of the bars
       CONFIG BONDSL
   2 NAME   "Interface2"                   Mid bars
       THICK   1.25600E+002                Circumference of the bars
       CONFIG BONDSL
   3 NAME   "BotBar"
       CROSSE  8.04000E+002                Cross-section area
   4 NAME   "MidBar"
       CROSSE  2.01000E+002
   5 NAME   "DummySuspension"
       CIRCLE  1.50000E+002
   6 NAME   "Strength"
       CROSSE  6.28E+002
   7 NAME   "Concrete"
       THICK   3.50000E+002                Thickness
   8 NAME   "WoodBoard"
```

```
        THICK    3.50000E+002
    9 NAME     "SteelPlate"
        THICK    3.50000E+002
   10 NAME     "Stirrup"
        CROSSE   1.57000E+002
   11 NAME     "TopBar"
        CROSSE   4.02000E+002
   12 NAME     "Strengthening"  Only used when running  analysis without  bond
        CROSSE   0.00E+000              slip on  strengthening bars
   13 NAME     "Interface3"                       Strengthening bars
        THICK    5.02000E+001                      Circumference of the bars
        CONFIG BONDSL
'DATA'
   12 NAME     "DummySuspension"
    1 NAME     "Concrete"
   13 NAME     "WoodBoard"
   14 NAME     "SteelPlate"
    3 NAME     "BotBar"
    4 NAME     "MidBar"
   15 NAME     "Strength"
    2 NAME     "Interface"
   16 NAME     "Interface2"
    6 NAME     "Stirrup"
    8 NAME     "TopBar"
   10 NAME     "Strengthening"
   17 NAME     "Interface3"
```

Elements

```
'ELEMENTS'
CONNECT
4351 L8IF    508 155 4525 4524
4352 L8IF    3505 508 4526 4525
4353 L8IF    4081 3505 4527 4526
 .
 .
 .
5311 L8IF    4974 4975 3255 4290
5312 L8IF    4975 4976 4290 686
5313 L8IF    4976 4977 686 339
4466 L2TRU   4524 4525
4467 L2TRU   4525 4526
4468 L2TRU   4526 4527
 .
 .
 .
5349 L2TRU   4974 4975
5350 L2TRU   4975 4976
5351 L2TRU   4976 4977
   1 Q8MEM   1 4 5 2
   2 Q8MEM   2 5 6 3
   3 Q8MEM   4 7 8 5
 .
 .
 .
5197 Q8MEM   4896 4897 4886 4885
5198 Q8MEM   4898 4889 4878 4887
5199 Q8MEM   4899 4898 4887 4888
5127 L6BEN   91 4836
```

Interface elements

Reinforcement elements

2D elements, concrete, steel plate and wood board

Assignment of material, data and geometry for elements

```
MATERI
/ 1-4350 / 1                              Concrete
/ 4351-4465 4581-4695 / 2                 Interface
/ 4466-4580 4696-4810 / 3                 Reinforcement
/ 5127 / 6                                Dummy suspension
/ 5142-5169 / 7                           Wood board
/ 5170-5199 / 8                           Steel plate
/ 5238-5275 5314-5351 / 9                 Strengthening bars
/ 5200-5237 5276-5313 / 10                Int. for strength.
DATA
/ 5127 / 12
/ 1-4350 / 1
/ 5142-5169 / 13
/ 5170-5199 / 14
/ 4466-4580 / 3
/ 4696-4810 / 4
/ 5238-5275 5314-5351 / 15
/ 4351-4465 / 2
/ 4581-4695 / 17
/ 5200-5237 5276-5313 / 16
GEOMET
/ 4351-4465 / 1                           Int. for bot. bars
/ 5200-5237 5276-5313 / 2                 Int. for mid bar
/ 4466-4580 / 3                           Bot bars
```

```
/ 4696-4810 / 4                                        Mid bar
/ 5127 / 5                                             Dummy suspension
/ 5238-5275 5314-5351 / 6                              Strengthening bars
/ 1-4350 / 7                                           Concrete
/ 5142-5169 / 8                                        Wood board
/ 5170-5199 / 9                                        Steel plate
/ 4581-4695 / 13                                       Int. for strength.
```

Definitions and assignments of embedded reinforcement

```
'REINFORCEMENTS'
LOCATI
   1 BAR
     LINE    1101 1100
     LINE    1100 954
     LINE    954 1816
       .
       .
       .
   2 BAR
     LINE    3737 2754
     LINE    2754 3204
     LINE    3204 2371
       .
       .
       .
   3 BAR
     LINE    934 933
     LINE    933 932
     LINE    932 931
       .
       .
       .
   4 BAR
     LINE    2597 4539
     LINE    4539 2268
     LINE    2268 2592
       .
       .
       .
   5 BAR
     LINE    126 479
     LINE    479 3456
     LINE    3456 2543
       .
       .
       .
   6 BAR
     LINE    4756 4757
     LINE    4757 4758
     LINE    4758 4759
       .
       .
       .
   7 BAR
     LINE    4795 4796
     LINE    4796 4797
     LINE    4797 4798
```

```
        .
        .
        .
MATERI
/ 5 / 3
/ 1-4 / 4
/ 6 7 / 5
GEOMET
/ 1-4 / 10
/ 5 / 11
/ 6 7 / 12
DATA
/ 1-4 / 6
/ 5 / 8
/ 6 7 / 10
```

Definations of loads

```
'LOADS'
CASE 1
WEIGHT
2 -9.81000E+000          ⎫  Phase 1 self-weight applied
:CASE 2                  ⎭
:DEFORM                  ⎫
:4892 TR 2 -1.00000E+000 ⎬  Phase 2 load applied with deflection control
'GROUPS'                 ⎭
ELEMEN
  12 "ConcreteBeam" / 1-4350 /
  18 "BotBar" / 4466-4580 /
  23 "MidInterface" / 4581-4695 /
  24 "MidBar" / 4696-4810 /
  25 "BotInterface" / 4351-4465 /
  34 "DummySuspension" 5127
  36 "WoodBoard" / 5142-5169 /
  37 "SteelPlate" / 5170-5199 /
  44 "Auto-Mesh(Face)" / 5200-5237 /
  45 "St1" / 5238-5275 /
  50 "Auto-Mesh(Face)-1" / 5276-5313 /
  51 "St2" / 5314-5351 /
```

Boundary conditions and constrains

```
'SUPPOR'
/ 121-159 4524 4640 / TR 1  ⎫
/ 121-159 4524 4640 / TR 3  ⎬  Supports in phase 1
/ 91 / TR 2                 ⎭
:/ 4892 / TR 2              ⎤  Node where deflection control is applied to
'TYINGS'
ECCENT TR 2
/ 94 88 97 85 100 82 103 79 76 106 / 91  ⎤  Tying of the support nodes
EQUAL TR 2
/ 4977 / 339  ⎫  Strengthening bars tied to the concrete at the
/ 4938 / 326  ⎭  top to represent the nuts
```

Units

```
'UNITS'
FORCE N      ⎫  Units are N and mm, that is recommended for
LENGTH MM    ⎬  two dimensional analysis
'END'        ⎭
```

Appendix C.   Command file for FE analysis

Command file for first phase

```
*FILOS
 INITIA
*INPUT
*PHASE
BEGIN ACTIVE
 ELEMENT ALL
 REINFO ALL
END ACTIVE
*NONLIN

 BEGIN TYPE
  BEGIN PHYSIC
   END PHYSIC
  END TYPE

 BEGIN OUTPUT
  FXPLUS
   FILE "1"
 END OUTPUT

 BEGIN EXECUTE
  BEGIN LOAD
   LOADNR=1
    BEGIN STEPS
     BEGIN EXPLIC
      SIZES 1.0(1)
     END EXPLIC
    END STEPS
   END LOAD
   BEGIN ITERAT
     METHOD NEWTON REGULA
:     METHOD SECANT BFGS
```

Output saved in file 1 for the first phase

Self weight

Applied in one step

Iteration method

```
      MAXITE=100
:      LINESE
      BEGIN CONVER
        ENERGY CONTIN TOLCON=0.0001  ⎤
        FORCE CONTIN TOLCON=0.01     ⎬─  **Convergence criteria**
        DISPLA CONTIN TOLCON=0.01    ⎦
      END CONVER
     END ITERAT
     SOLVE GENEL
   END EXECUT
*END
```

Command file for second phase

```
*INPUT
READ TABLE LOADS
READ TABLE SUPPORTS
READ TABLE TYINGS
*PHASE
BEGIN ACTIVE
 ELEMENT ALL
 REINFO ALL
END ACTIVE
*NONLIN

  BEGIN TYPE
  BEGIN PHYSIC
:     INTERF ON
:     TOTCRK ON SECANT
   END PHYSIC
  END TYPE


BEGIN OUTPUT       ⎤
  FXPLUS FXPLUS    ⎬   **Output saved in file 2 for the second phase**
  FILE "2"         ⎦
 END OUTPUT
```

```
BEGIN EXECUTE
  BEGIN LOAD
   LOADNR=1                                         Self-weight
    BEGIN STEPS
     BEGIN EXPLIC
      SIZES 1.0(1)
     END EXPLIC
    END STEPS
   END LOAD
   BEGIN ITERAT
     METHOD NEWTON REGULA
:     METHOD SECANT BFGS
     MAXITE=100
:     LINESE
     BEGIN CONVER
       ENERGY CONTIN TOLCON=0.0001
       FORCE CONTIN TOLCON=0.01
       DISPLA CONTIN TOLCON=0.01
     END CONVER
   END ITERAT
   SOLVE GENEL
  END EXECUT


  BEGIN EXECUTE
  BEGIN LOAD
   LOADNR=2                                         Load 2 deflection control
    BEGIN STEPS
    BEGIN EXPLIC
     SIZES 0.05(26)                                 Applied in steps
    END EXPLIC
    END STEPS
   END LOAD
   BEGIN ITERAT
    CONTIN
```

```
      METHOD NEWTON REGULA
:     METHOD SECANT BFGS
      MAXITE=350
:     LINESE
      BEGIN CONVER
        ENERGY CONTIN TOLCON=0.0001
        FORCE CONTIN TOLCON=0.01
        DISPLA CONTIN TOLCON=0.01
      END CONVER
    END ITERAT
    SOLVE GENEL
  END EXECUT
```

Unloading phase

```
  BEGIN EXECUTE
   BEGIN LOAD
   LOADNR=2
    BEGIN STEPS
     BEGIN EXPLIC
     SIZES -0.05(25)                                      Unloading
    END EXPLIC
    END STEPS
   END LOAD
    BEGIN ITERAT
     CONTIN
     METHOD NEWTON REGULA
:     METHOD SECANT BFGS
     MAXITE=350
:     LINESE
      BEGIN CONVER
        ENERGY CONTIN TOLCON=0.0001
        FORCE CONTIN TOLCON=0.01
        DISPLA CONTIN TOLCON=0.01
      END CONVER
    END ITERAT
```

```
    SOLVE GENEL
  END EXECUT


 BEGIN EXECUTE
 BEGIN LOAD
  LOADNR=2
   BEGIN STEPS
    BEGIN EXPLIC
    SIZES 0.05(200)                        Loaded up to failure
   END EXPLIC
   END STEPS
  END LOAD
  BEGIN ITERAT
    CONTIN
    METHOD NEWTON REGULA
:    METHOD SECANT BFGS
    MAXITE=350
:    LINESE
    BEGIN CONVER
      ENERGY CONTIN TOLCON=0.0001
      FORCE CONTIN TOLCON=0.01
      DISPLA CONTIN TOLCON=0.01
    END CONVER
  END ITERAT
  SOLVE GENEL
 END EXECUT
```

Appendix D.   Set up of LVTD:s

M5

ABOVE

UNDER
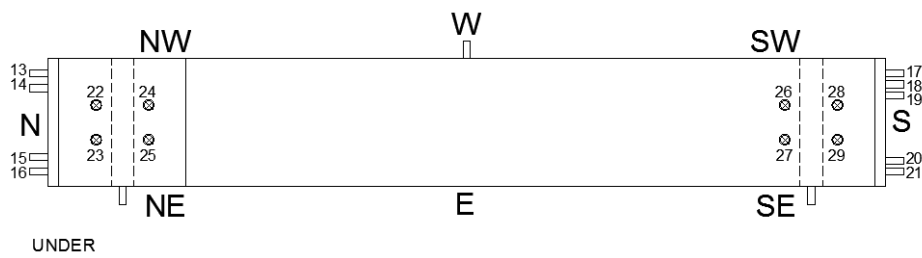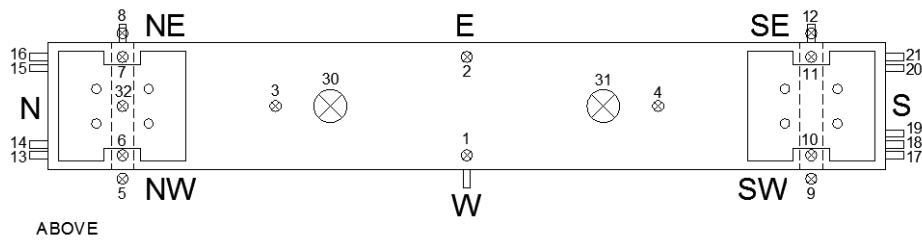
M9

LVTD number 19 and 33 are positioned on the concrete

ABOVE

UNDER
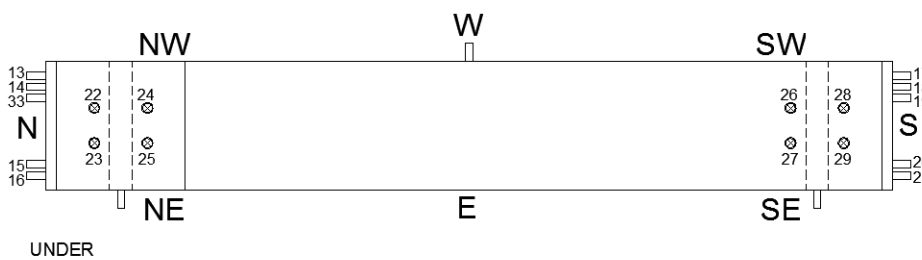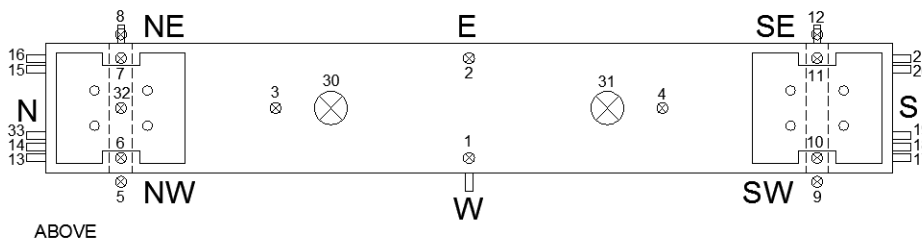
Appendix E.   Documentations   of   specimens   before testing

R6
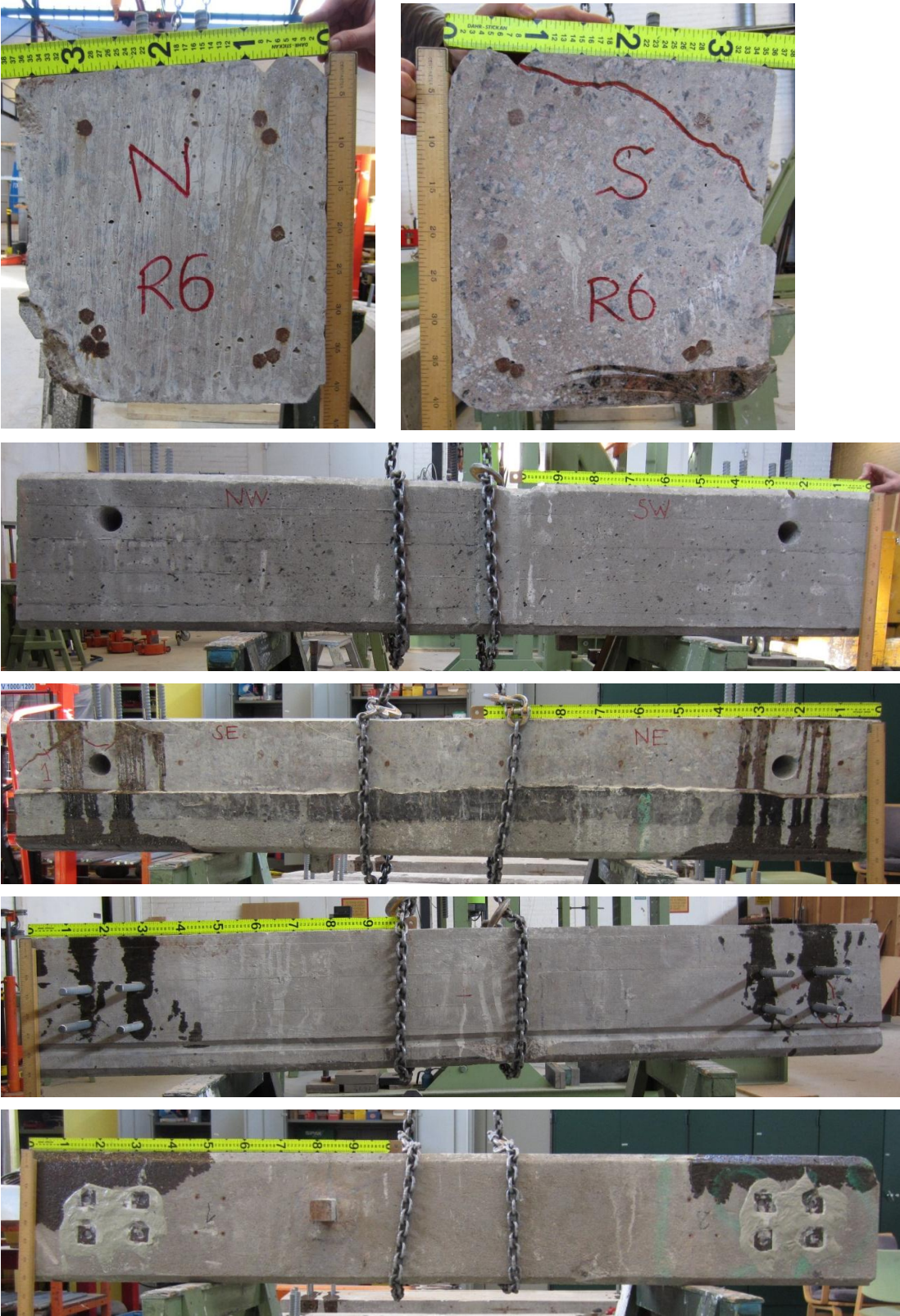
M4

M5
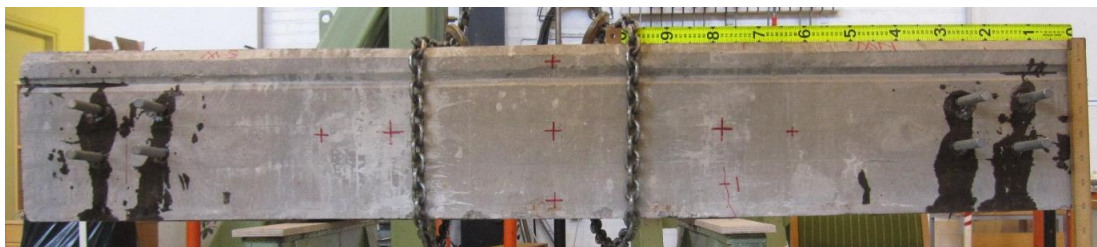
M6
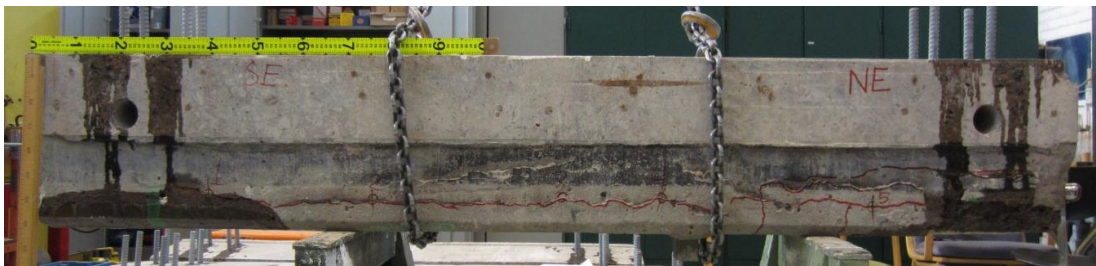
M9
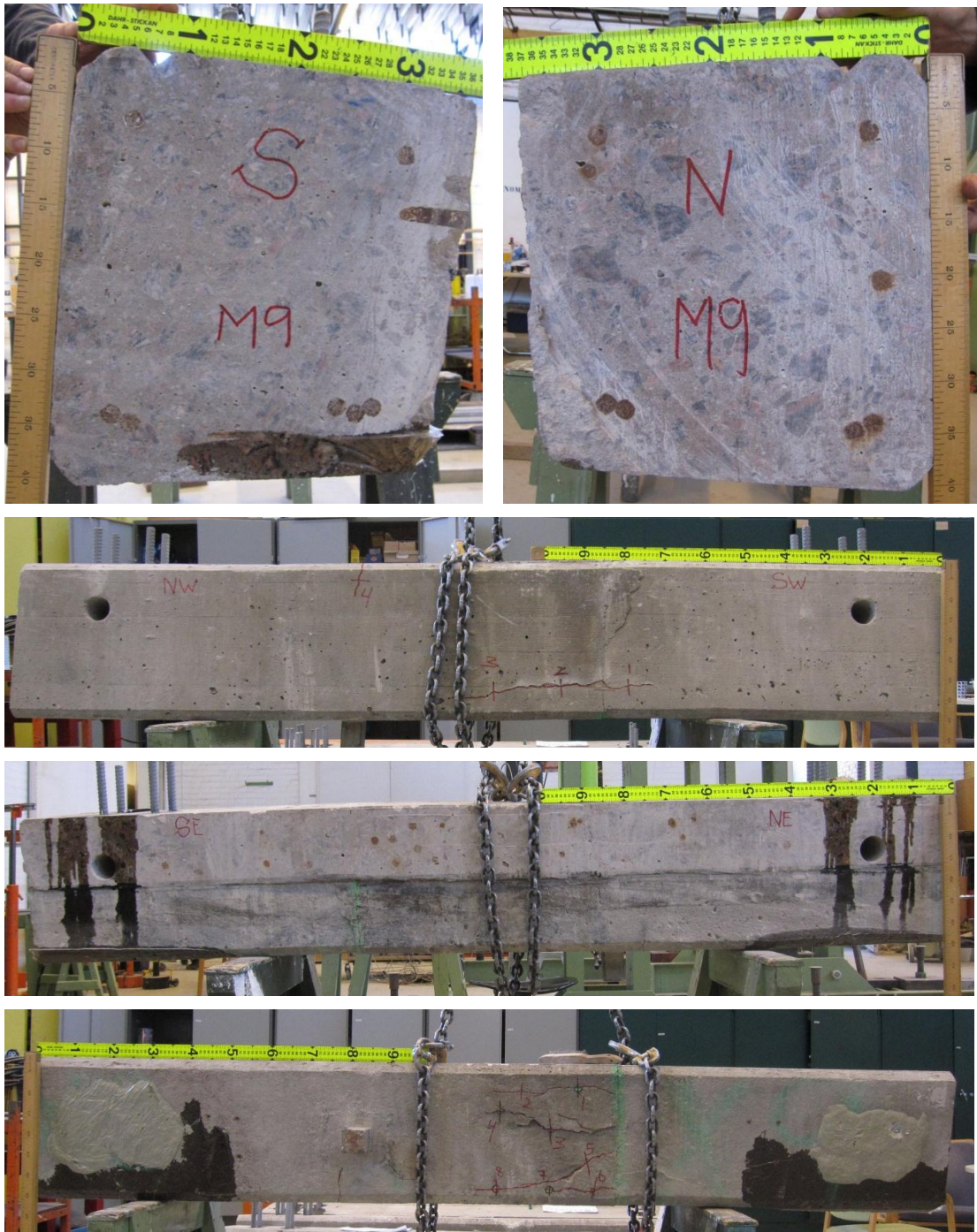
Appendix F.   Crack widths and locations before testing

Instructions for documentations

Documentation of the crack width and the crack pattern:

1. Mark the length of the specimens 2.3 meter and highlight the label with green paint.
2. Mark the position of crack width measurements with black marker and number them as 1, 2, 3, ...
3. **Photo-1:** a complete beam
4. **Photo-2:** Take a photo from both end cross sections.
5. Put the 3 rulers on the left half of the beam.
6. **Photo-3:** just left half of the beam.
7. **Photo-4:** left half on top
8. **Photo-5:** each point for crack width measurement are photographed one by one on left half on top
9. **Photo-6:** left half on the two sides (left half of the beam)
10. **Photo-7:** each point for crack width measurement are photographed one by one on left half on side
11. Do steps 4 to 9 for the right side of the beam
12. Measure crack width of the points and write the values in the following tables:

M4

Date: 26 /03 /2012   Inspector: EG&TG   Beam No.: M4

North edge of the beam:

Bottom (NU)   Side 1(NE)   Side 2(NW)

No.	X	Y	Crack width (mm)
1			
2			
3	75	12	0.1
4	58	19	0.1
5			
6			
7			
8			
9			
10			

No.	X	Y	Crack width (mm)
1			
2			
3	91	30	1.5
4	64	30	1.5
5			
6	23	32	?
7	7	29	1.4
8			
9			
10			

No.	X	Y	Crack width (mm)
1	96	7	0.4
2	97	20	0.1
3			
4			
5			
6			
7			
8			
9			
10			

South edge of the beam:

Bottom (SU)   Side 1(SE)   Side 2(SW)

No.	X	Y	Crack width (mm)
1	75	5	0.1
2	87	5	0.1
3			
4			
5			
6			
7			
8			
9			
10			

No.	X	Y	Crack width (mm)
1	80	30	2
2	109	31	2.5
3			
4			
5	126	20	1.4
6			
7			
8			
9			
10			

No.	X	Y	Crack width (mm)
1			
2			
3			
4			
5			
6			
7			
8			
9			
10			

Notes: ....

M5

North edge of the beam:

Bottom (ND)

No.	X	Y	Crack width (mm)
1	79	30	0.1
2			
3			
4			
5			
6			
7			
8			
9			
10			

Side 1(NE)

No.	X	Y	Crack width (mm)
1	48	31.5	0.1
2	62	30	0.1
3	83.5	33	0.5
4	83	35	0.3
5			
6			
7			
8			
9			
10			

Side2(NW)

No.	X	Y	Crack width (mm)
1	73	7	0.5
2	84.5	33	0
3	85	22.5	0.3
4	90	12	0.5
5	97.7	29.5	0.2
6			
7			
8			
9			
10			

South edge of the beam:

Bottom (NU)

No.	X	Y	Crack width (mm)
1	37	28	0.2
2	59	26	0.6
3	69	26	0.5
4			
5			
6			
7			
8			
9			
10			

Side 1(SE)

No.	X	Y	Crack width (mm)
1			
2			
3			
4			
5	55	28	0.4
6	32	25.5	0.1
7	26	31	0.6
8	12	31	0.5
9			
10			

Side2(SW)

No.	X	Y	Crack width (mm)
1			
2			
3			
4			
5			
6	61.5	33.5	0.3
7	62	25	0.3
8			
9			
10			

Notes: ....

M6

Date: 28 /03 /2012   **Inspector:EG & TG**   **Beam No.: M6**

North edge of the beam:

Bottom (NU)

No.	X	Y	Crack width (mm)
1			
2	72	6	0.2
3	57	10	2
4			
5			
	Top (NT)		
1	85	8	0.2
2	81	33	0.4
3			
4			

Side 1(NE)

No.	X	Y	Crack width (mm)
1			
2			
3	114	30	1.1
4	93	29	3.2
5	46	31	0.8
6			
7			
8			
9			
10			

Side 2(NW)

No.	X	Y	Crack width (mm)
1	80	4.5	0.4
2			
3			
4			
5			
6			
7			
8			
9			
10			

South edge of the beam:

Bottom (SU)

No.	X	Y	Crack width (mm)
1	107	20	0.4
2			
3			
4			
5			
6			
7			
8			
9			
10			

Side 1(SE)

No.	X	Y	Crack width (mm)
1	39	29	1.5
2	75	30	3.0
3			
4			
5			
6			
7			
8			
9			
10			

Side 2(SW)

No.	X	Y	Crack width (mm)
1			
2	95	4	0.3
3			
4			
5			
6			
7			
8			
9			
10			

Notes: ....

M9

North edge of the beam:

Bottom (NU)

No.	X	Y	Crack width (mm)
1			
2			
3			
4			
5			
6			
7			
8			
9			
10			

Side 1(NE)

No.	X	Y	Crack width (mm)
1			
2			
3			
4			
5			
6			
7			
8			
9			
10			

Side2(NW)

No.	X	Y	Crack width (mm)
1			
2			
3			
4			
5			
6			
7			
8			
9			
10			

South edge of the beam:

Bottom (SU)

No.	X	Y	Crack width (mm)
1	95	6	0.6
2	108	7	0.3
3	109	16	0.5
4	114	11	0.3
5	92	24	0.3
6	90	32	0.4
7	102	32	0.1
8	115	32	0.5
9			
10			

Side 1(SE)

No.	X	Y	Crack width (mm)
1			
2			
3			
4			
5			
6			
7			
8			
9			
10			

Side2(SW)

No.	X	Y	Crack width (mm)
1	79	32.5	0.2
2	96	32	2.0
3	111	33.5	0.5
4	86	5	0.4
5			
6			
7			
8			
9			
10			

Notes: Concrete joint crack width is around 0.1-1.0mm

R6

Date 28 / 03 / 2012   Inspector: EG & TG   Beam No: R6

North edge of the beam:

Bottom (NU)   Side 1(NE)   Side 2(NW)

No.	X	Y	Crack width (mm)
1			
2			
3			
4			
5			
6			
7			
8			
9			
10			

No.	X	Y	Crack width (mm)
1			
2			
3			
4			
5			
6			
7			
8			
9			
10			

No.	X	Y	Crack width (mm)
1			
2			
3			
4			
5			
6			
7			
8			
9			
10			

South edge of the beam:

Bottom (SU)   Side 1(SE)   Side 2(SW)

No.	X	Y	Crack width (mm)
1			
2			
3			
4			
5			
6			
7			
8			
9			
10			

No.	X	Y	Crack width (mm)
1	10	9	1
2			
3			
4			
5			
6			
7			
8			
9			
10			

No.	X	Y	Crack width (mm)
1			
2			
3			
4			
5			
6			
7			
8			
9			
10			

Notes: ....

Appendix G. Documentations of specimens after testing
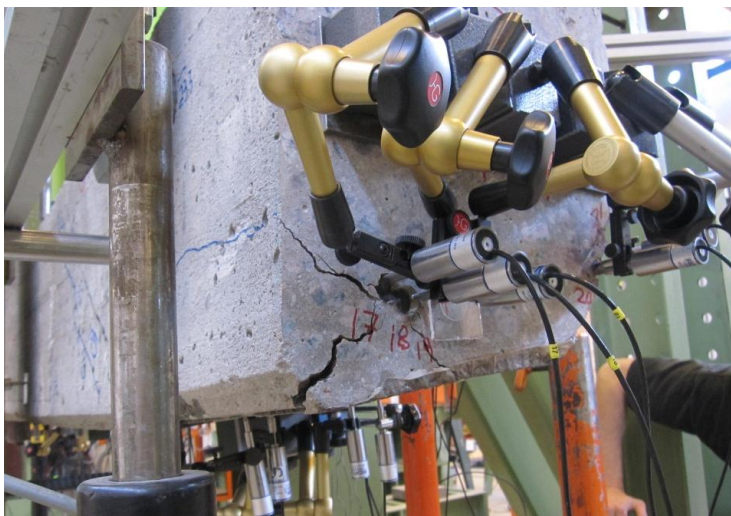
M4

East side

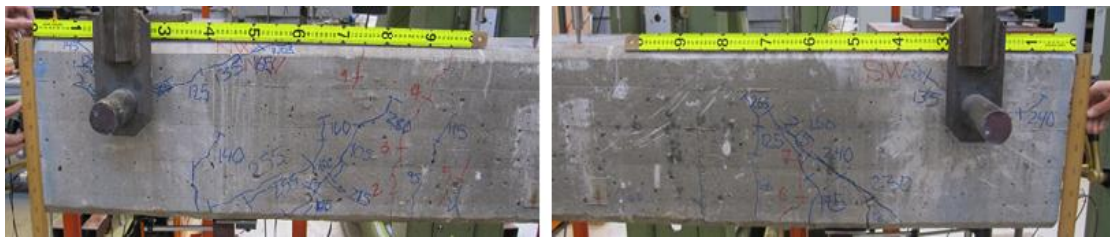West side

Failure end

M5
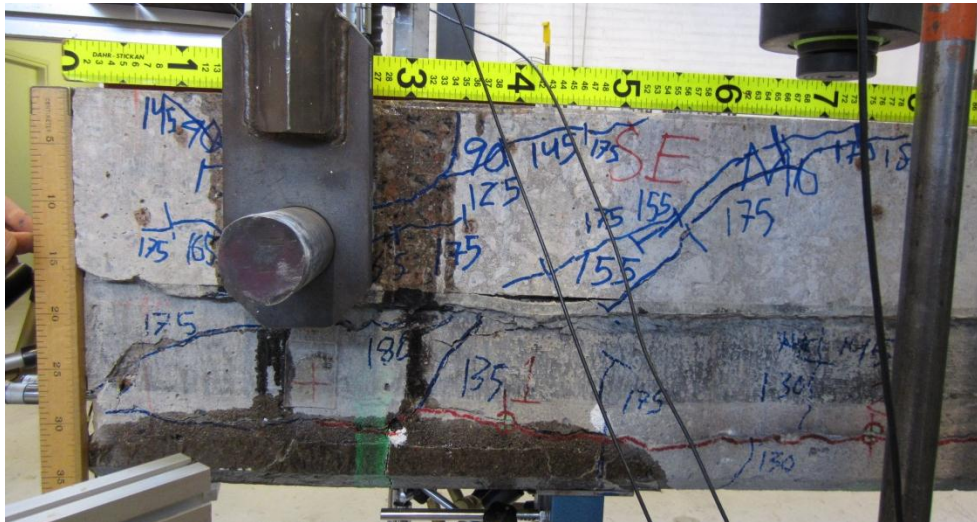
East side

West side

Crack pattern on bottom on south side (failure side)

M6

East side

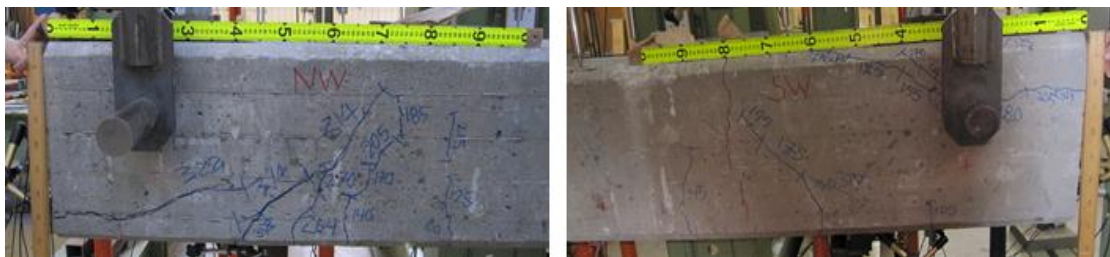West side

M9

East side

West side

Failure end (south end)

R6

East side

West side

Failure end (north end)